EFFECTS OF RESONANT VIBRATIONS ON DROPLETS FOR ENHANCED DROPWISE CONDENSATION

A Thesis

by

SAROJEET BHAKTIBHUSHAN DEB

Submitted to the Office of Graduate and Professional Studies of
Texas A&M University
in partial fulfillment of the requirements for the degree of

MASTER OF SCIENCE

Chair of Committee,	Jorge L. Alvarado
Co-chair of Committee,	Michael Pate
Committee Members,	M. Cynthia Hipwell
	Mark Kimber
Head of Department,	Andreas A. Polycarpou

December 2019

Major Subject: Mechanical Engineering

ABSTRACT

In order to improve dropwise condensation (DWC), droplets must be efficiently shed from the surface to avoid a film formation and low heat transfer rates. Coatings and nanostructured surfaces have been used to achieve better droplet shedding, but they face problems of poor long-term durability and affordability. Thus, active methods relying on external stimuli must be explored.

A vibration study using three substrates (copper, PTFE and Saphir) was undertaken to understand the effects of vibration parameters on droplet mobility. The substrates ranged from being hydrophilic to hydrophobic. The first objective was to determine the resonant frequencies of droplets on these surfaces for a range of droplet sizes, ranging from 3.3 μl to 6.8 μl. The experimental resonant frequencies were measured and compared to the ones obtained from the Celestini's model for validation purposes. A discrepancy of about 20 % was observed.

In the next part of the study, the droplets were vibrated with increasing accelerations until sliding was observed. The acceleration and frequency at sliding were recorded, and the amplitude and vibration intensity was calculated. These parameters were compared across each surface and droplet volume.

In all the experiments, it was noticed that amplitude, acceleration, and vibration intensity depended on droplet volume and the hydrophobicity of the surface. Droplets of smaller volume needed greater vibrational energy to slide due to relatively high

magnitude of the corresponding adhesive force. For droplets of the same volume, it was observed that hydrophobic substrates are better than hydrophilic substrates in promoting sliding. It was also observed that roughness of the substrate plays a significant role in reducing the sliding of the droplet.

Finally, across any droplet size-substrate combination, it was observed that vibrations at resonant frequency of the droplet led to easier sliding with the least consumption of energy, as indicated by the vibration intensity. Thus, it is advisable to use resonant frequency of droplets to promote droplet shedding in a host of applications including dropwise condensation.

DEDICATION

This work is dedicated to my late sister, Aparna di. You are the reason of my every success, and I miss you a lot. May your soul rest in peace.

ACKNOWLEDGEMENTS

I would like to thank my committee chair, Dr. Jorge Alvarado, who believed in my ability to perform research and provided the encouragement I needed to graduate on time. I would also like to thank my committee members and faculty, Dr. Michael Pate, Dr. Cynthia Hipwell and Dr. Mark Kimber for their guidance and support throughout the course of this research. I would also like to thank the departments of Mechanical Engineering and Engineering Technology and Industrial Distribution for their financial and infrastructural support.

I would like to thank my family – Mom, sister Arati and brother-in-law Vijay. I would also like to thank my friends and labmates – Aparna, Rohan, Hardik, Shitiz, Zaki, Shantanu, Mayur, Kalpak, Xiaoyu and Yi, who helped me maintain my mental well-being through this arduous phase of research.

I would also like to thank the Tata Trust and K.C. Mahindra Education Trust for their generous scholarships.

CONTRIBUTION AND FUNDING SOURCES

I would like to acknowledge the contribution of my committee members Dr. Jorge Alvarado, Dr. Michael Pate, Dr. Cynthia Hipwell and Dr. Mark Kimber. I would also like to acknowledge the contribution of my labmates and former students from the lab, Dr. Chun-Wei Yao, Yi Wang and Xiaoyu Hu. The project was funded through the PI Incentive account of Prof. Alvarado.

NOMENCLATURE

θ	Contact angle
θ_a	Advancing angle
θ_r	Receding angle
$\Delta\theta$	Contact angle hysteresis
$\frac{F}{l}$	Pinning force per unit length
a	Acceleration
f	Frequency
u_o	Spatial displacement of substrate
g	Gravitational acceleration
j	Resonance mode
m	weight of the droplet
p	Half arc length of a droplet
q_j	Wave factor for one dimensional capillary-gravity wave
R	Droplet radius
V	Droplet volume
γ	Surface tension
ρ	Density of droplet
ω	Resonance frequency
δ	Stoke's length

μ	Kinematic viscosity

Subscript:

j	Resonance mode
L	Liquid
S	Solid
V	Vapor

TABLE OF CONTENTS

Page

LIST OF FIGURES

Page

LIST OF TABLES

Page

1. INTRODUCTION AND LITERATURE REVIEW

1.1 Condensation

Condensation is an important two-phase heat transfer phenomenon in the study of heat transfer. It occurs in many applications including cooling towers of power plants to heat pipes in electronics systems. Condensation occurs when the temperature of a condensable vapor is reduced below its saturation temperature, often due to contact with a cold surface, resulting in the formation of condensate. Due to condensation, the latent heat of the vapor is released, which is significant due to the large internal energy differences between the liquid and vapor states [1]

Condensation may occur in the presence of non-condensable gases like air, or lack thereof. Non-condensable gases provide high thermal resistance to condensation, as demonstrated by Al-Shammari [2]. The condensation heat transfer increases with an increase in mass fraction of condensable gases [3]. Irrespective of the presence of non-condensable gases, there are two main modes of condensation. The most commonly observed one is filmwise condensation (FWC), where a liquid film wets the surface. The film usually grows in thickness along the length of the surface and forms a blanket. Filmwise heat transfer usually occurs on clean and uncontaminated surface. If the liquid poorly wets the surface, droplets may form, leading to Dropwise Condensation (DWC). However, dropwise condensation (DWC) occurs at a specific temperature range or under different wetting conditions even without the onset of filmwise condensation. In

dropwise condensation (DWC) there are four prevalent phases, including, nucleation, growth, coalescence and shedding of droplets. The droplets originate at the points of imperfections called nucleation sites. They grow in size due to absorption of vapor and may coalesce with other droplets. Finally, these droplets roll down the surface under the influence of gravity, paving the way for nucleation of future droplets. The difference between filmwise and dropwise condensation is shown in Fig. 1.1. Since the wettability of the surface plays an important role in deciding the mode of heat transfer, understanding the concept of wettability would be useful.

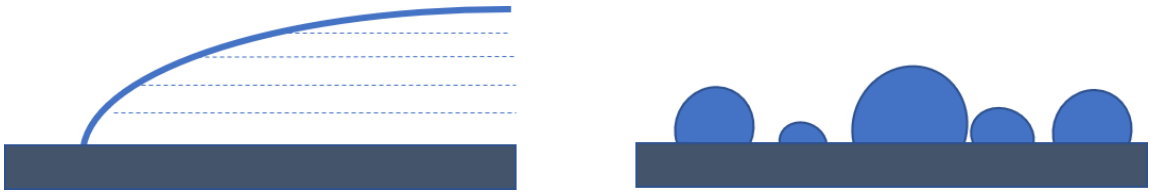

Figure 1.1: Filmwise and dropwise condensation

1.2 Droplet behavior on surfaces

In the study of droplet wettability on condensation surfaces, there are certain parameters that should be studied and analyzed. Among the physical parameters used in the study of droplet wettability, contact angle is one of the most important ones since it is usually independent of droplet volume. Contact angle is defined as the angle made by the liquid vapor interface of a droplet with the solid surface. It is also used to quantify the wettability of a surface by a liquid. Depending on the value of contact angle, there

are two types of surfaces. Hydrophilic surfaces have a static contact angle of less than 90°, while hydrophobic surfaces have a static water contact angle more than 90°, as shown in Fig. 1.2.

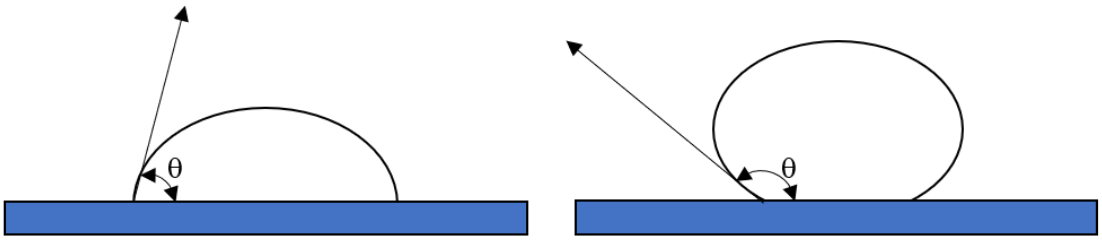

Figure 1.2: Droplet contact angle on hydrophilic and hydrophobic surfaces

When a droplet slides or is tilted while sitting on a surface, it would deform accordingly. On the front side of the droplet, the contact angle is usually greater than on the backside. The contact angle on the front side of the droplet is called advancing contact angle, θ_A, while on the backside is called receding angle, θ_R as shown in Fig. 1.3. Both these angles are a characteristic of surface chemistry and topography. The difference between advancing and receding angles is called contact angle hysteresis [4].

$$\Delta\theta = \theta_a - \theta_r \tag{1.1}$$

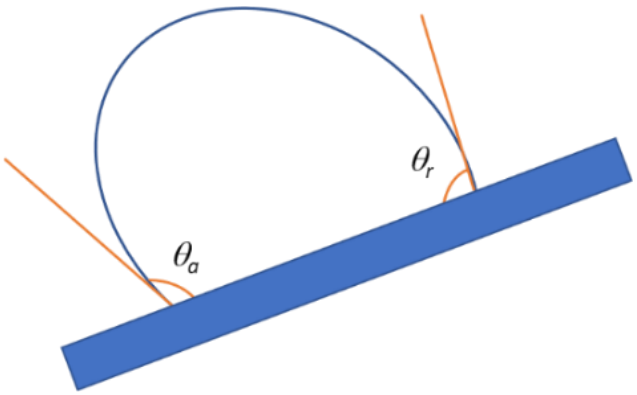

Figure 1.3: Advancing and receding angle on a droplet

Another physical parameter used in wettability studies is surface energy. For a liquid in contact with a solid, surface energy is defined as the product of surface tension and contact area. Thus, the energy required to create a unit area of interphase is called surface tension (γ) [5]. Young's equation [6] gives the following relation between static contact angle (θ) and surface tension (γ) for a droplet at static equilibrium:

$$\cos\theta = \frac{\gamma_{SV} - \gamma_{SL}}{\gamma_{LV}} \tag{1.2}$$

where γ_{SV}, γ_{SL}, and γ_{LV} are the surface tension between the solid and vapor phases, solid and liquid phases, and liquid and vapor phases respectively, as shown in Fig. 1.4.

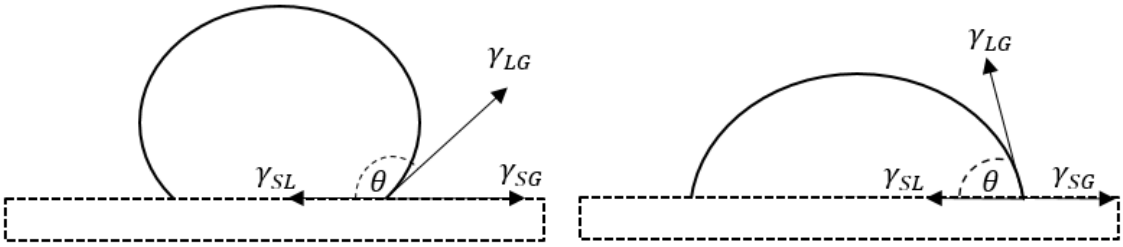

Figure 1.4: Surface tension forces acting on a drop on a hydrophobic and hydrophilic surface

1.3 Techniques for promoting DWC over FWC

In FWC, the liquid film exhibits greater thermal resistance to heat transfer than in DWC. On the other hand, in DWC the condensing vapor can directly lose its heat to a large portion of the exposed dry surface, instead of interacting with the liquid film or existing droplets. Moreover, the thermal resistance associated with small droplets is usually smaller than the one found in liquid films. Thus, surface heat transfer coefficient in DWC is usually an order of magnitude greater than FWC, and thus is the preferred mode of condensation heat transfer.

The phenomenon of condensation finds most of its applications in condensers, which range from hand-held ones to massive ones used in power plants. Condensers are usually made from high conductivity metals like copper or aluminum. Clean metals are generally hydrophilic in nature, and thus it is difficult to achieve efficient droplet shedding due to the inherent low contact angle that droplets make on the surface. Thus, active and passive techniques have been developed to enhance DWC.

1.3.1 Passive techniques

Passive techniques do not involve use of external energy to promote DWC. Changes can be made either to the surface, by using coatings, ion implantations, nanostructures or liquid infused surfaces (LISs). Additives can be used in the condensing vapor to enhance wettability of the liquid on the surface [7].

Coatings have been explored by researchers for decades with the main goal of making surfaces hydrophobic to prevent liquid film formation. In 1968, Erb *et al.* [8] suggested the use of a variety of surface coatings like sulfides and selenides of copper and silver, noble metals like gold, silver, rhodium, palladium and platinum, as well as polymer films. Das *et al.* [9] used self – assembled monolayers (SAMs) on gold, copper and copper- nickel alloy surfaces to promote DWC of steam. Torresin *et al.* [10] used copper nanostructured surfaces in their flow condensation experiments.

Similar experiments involving rare earth oxides [11, 12], ion implantation [13], lubricant infused surfaces (LISs) [14] and graphene coatings [15] have been performed by researchers to enhance DWC. However, they are not durable enough for industrial applications and lose their performance gradually. For example, the hydrophilic base metal may diffuse to the surface [8] or the hydrophobic monolayer may degrade [10] or the lubricant may deplete from LISs [14].

1.3.2 Active techniques

Since passive techniques like coatings exhibit durability issues, different active methods to promote enhanced droplet shedding have been looked into, including electrohydrodynamic fields (EHD) [16-18] and bulk vibrations [19].

1.3.2.1 Electrohydrodynamic fields

Velkoff and Miller [18] were one of the initial researchers to explore EHD, as they observed heat transfer improvements of up to 150 % in condensation of Freon 114 vapor on cooled vertical copper plate. Didkovsky and Bologa observed heat transfer enhancement of up to 20 times during condensation of dielectric fluids on cooled vertical copper plate [16]. Laohalertdecha *et al.* [17] did a comprehensive review of 24 cases where EHD was used to enhance condensation heat transfer. They found the following mechanisms responsible for EHD enhancement:

- Thinning of condensate film due to depletion of liquid from condensation surface
- FWC changing to pseudo-DWC
- Perturbance of condensate film by electrostatic atomization
- Disturbing non-condensable gases at the liquid vapor interface

Although EHD seems promising, it requires a fluid with low electrical conductivity like refrigerants [20]. Thus, water cannot be condensed efficiently using EHD and so bulk vibrations should be considered.

1.3.2.2 Bulk vibrations

Yamali *et al.* [21] performed condensation experiments in the presence of non-condensable gases on a gold plated condenser surface mounted on a centrifuge. The centrifugal force is parallel to the condenser surface. They observed that as the acceleration increases, the dropwise heat transfer coefficient increased by an average of 0.27 power of the body force.

One of the first instances of increased heat transfer due to vibrations was observed at Southwest Research Institute by Raben *et al.* [22]. They used vibrations to increase evaporator performance in saline water conversion systems. It was found that beyond a threshold value, the heat transfer coefficient increased with vibration intensity up to a maximum of 55 % compared to vibration free case. They also observed that water did not completely shed the tube as one may imagine, instead it swayed from side to side which led to liquid accumulation.

Dent *et al.* [23] did an exploratory study on the condensation of steam in a horizontal condenser tube, which was vibrating in the plane of gravity. He conducted experiments in the 20 – 80 Hz range with an amplitude of 4.32 mm (0.17 in). He observed a maximum heat transfer increase of 15 %, which was dependent upon the amplitude of vibration. He also presented a mathematical model [24] which could calculate the heat transfer coefficient for FWC on a vertical tube vibrating transversely.

Migliaccio [19] investigated the effect of vertical vibration on condensation rates of water vapor on hydrophobic surfaces. Water vapor was condensed on a hydrophobic

surface cooled with miniature thermoelectric coolers and vibrated using piezoelectric actuators. Effect of vibrations of different frequencies ranging from 100 Hz – 400 Hz was investigated. He observed that due to vibrations, droplets departed the vertical surface before reaching the critical departure radii. He also observed that the lowest radii droplets departing for each vibration frequency corresponds to those droplets for which the rocking mode resonance frequency is close to the applied frequency. Vibrations also helped in reducing droplet size distributions, which implied that the number of larger, thermally inefficient droplets was reduced. Finally, he observed an increase in heat transfer rates of over 70%, compared to the stationary case.

As shown in previous studies, bulk vibrations have been proven useful to improve DWC. However, it is important to understand the different types of vibrations as well as the effects of vibrations on droplets.

1.4 Types of vibrations

There are two types of vibrations a droplet may experience, depending on the direction of vibration of the surface. They are longitudinal and lateral vibrations. Rahimzadeh *et al.* [25] presented a good distinction between longitudinal vibrations and lateral vibrations.

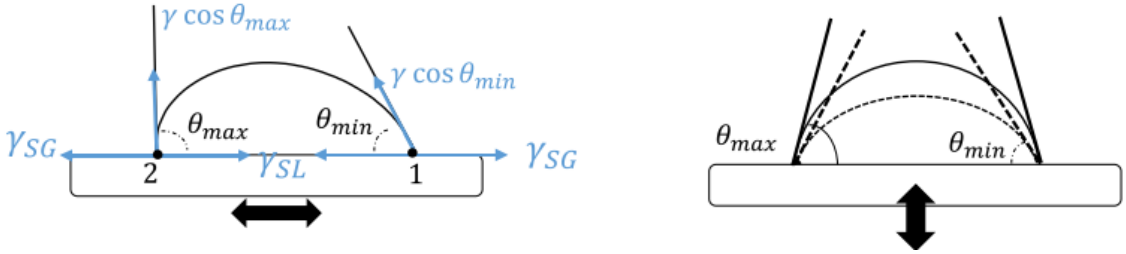

Figure 1.5: Difference between lateral and longitudinal vibrations. Reprinted from [25]

The difference between longitudinal and lateral vibrations of a droplet on a horizontal surface are shown in Fig 1.6. In summary, when a surface vibrates laterally, droplets experience rocking oscillations, in which the advancing and receding angles of the droplet attain maximum and minimum values, respectively. The maximum and minimum pinning forces per unit length is given by:

$$\frac{F_1}{l} = \gamma \cos \theta_{min} + \gamma_{SL} - \gamma_{SG} \tag{1.3}$$

$$\frac{F_2}{l} = \gamma \cos \theta_{max} + \gamma_{SL} - \gamma_{SG} \tag{1.4}$$

where 1 and 2 are two diametrically opposite points. Since $\frac{F_1}{l} > \frac{F_2}{l}$, the contact line mobility and phase of oscillation will be different on left and right side of the droplet accordingly. The left and right contact angles oscillate out of phase with each other. If this lateral vibration occurs on a vertical surface, the droplet starts drifting downwards if the acceleration is sufficient to overcome the yield force. Compared to lateral vibrations, a droplet oscillating under the influence of longitudinal vibrations shows simultaneous and in-phase fluctuations of left and right contact angles. This is shown in Fig. 1.5.

Now that the distinction between both this type of vibrations is clear, various studies on each type of vibration, along with their resonance modes, can be discussed.

1.5 Effects of longitudinal vibration on droplets

Andrieu *et al.* [26] used longitudinal vibrations on a horizontal surface to unpin free the contact line of droplets from surface defects. They found out that as amplitude of vibrations was increased, the contact angle hysteresis reduced, tending to zero. They also found a relation between the contact angle, advancing and receding contact angles after the droplets were unpinned, as follows:

$$\cos\theta = \frac{1}{2}(\cos\theta_a + \cos\theta_r) \tag{1.5}$$

Thus, contact angle hysteresis is a manifestation of the energy barrier droplets need to overcome to slide off a surface. Also, it prevents or minimizes droplet instabilities or a persistent dynamic behavior.

Brunet *et al.* [27] demonstrated that liquid drops can move against gravity while placed on an inclined, vertically vibrating substrate. They found out ranges of frequencies and amplitudes for which drops started climbing. This motion was attributed to the averaged Young capillary forces and droplet inertia due to the motion of center of mass of the droplet. The data were compiled into a map to indicate different regions of droplet being static, climbing or sliding. Fig. 1.6 represents one such map for V =5 µl, α =45° and v =31 mm^2/s. A similar work was done by Sartori *et al.* [28] for different liquids and substrates. In Fig 1.7, a droplet of volume of 2 µl at an inclination of 30° is considered. The normalization factors are a_o= 241 m s^{-2} and f_o= 70 Hz for water on PMMA and a_o=

110 m s^{-2} and f_o= 47 Hz for water on silanized PMMA. For the other liquids they are comprised in the ranges a_o=117–173 m s^{-2} and f_o=48−59 Hz.

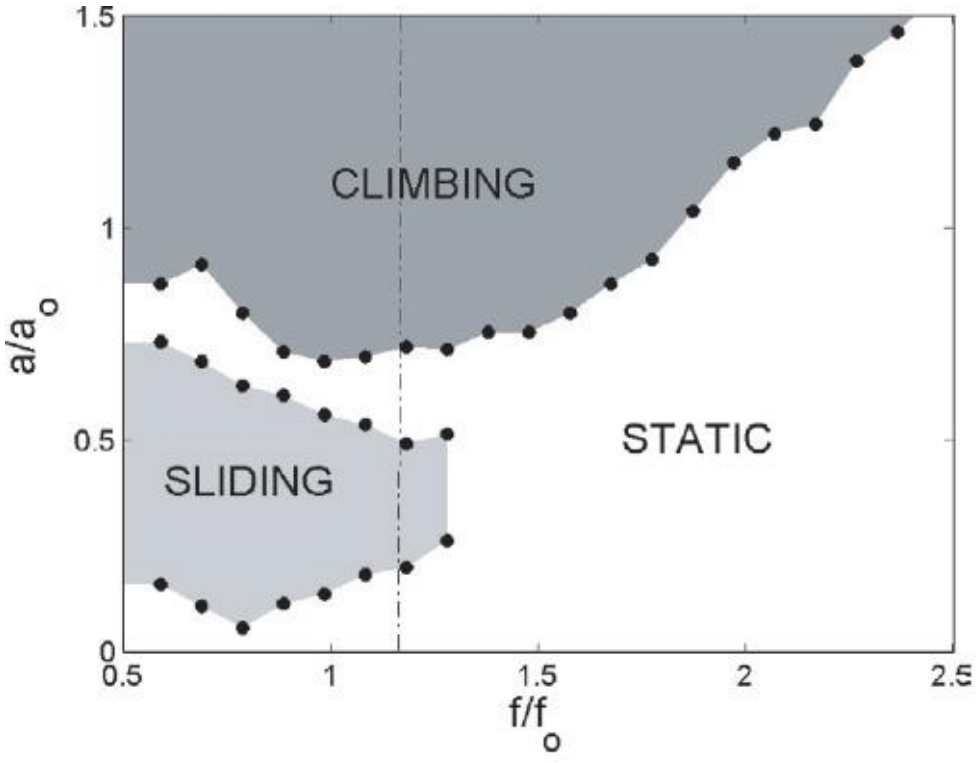

Figure 1.6: Acceleration and frequency dependence for droplet motion – static, climbing and sliding. Reprinted from [27]

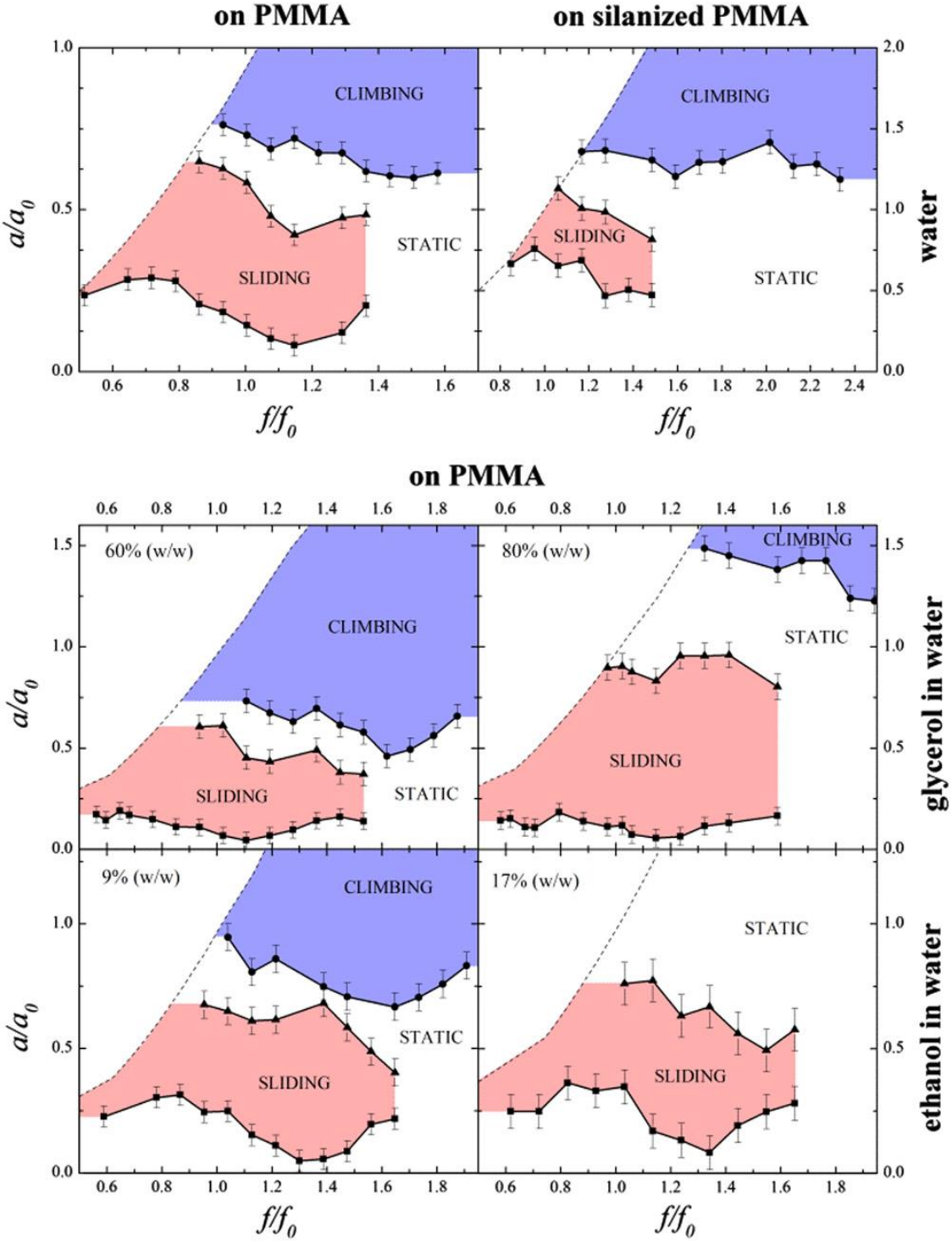

Figure 1.7: Acceleration and frequency dependence for droplet motion – static, climbing and sliding. Reprinted from [28].

Since vibrations at resonance frequencies have been shown to be highly effective in inducing droplet movement, several authors have attempted to formulate models that can predict the resonant frequency of droplets. Noblin and Brochard-Wyart [29] discovered the various vibration modes of a droplet. The first and second resonance modes, with two and four nodes respectively, are shown in Fig. 1.8.

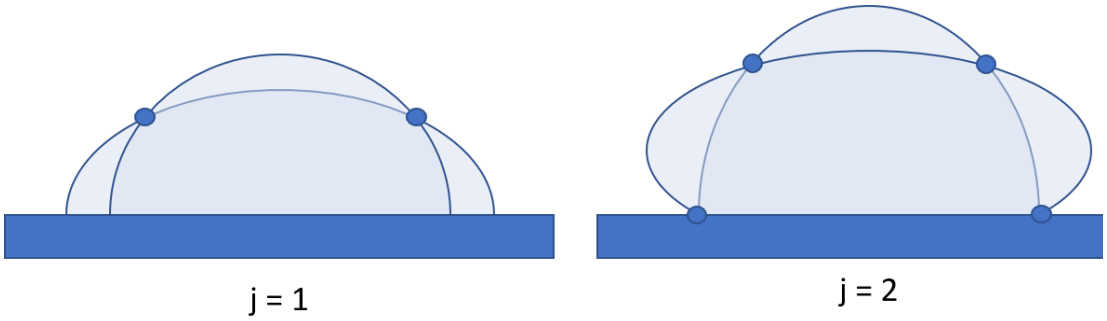

Figure 1.8: Modes of vibration of a droplet on a surface vibrating vertically

They also studied the effects of vertical oscillations on large sessile water drops. They found two modes of vibration, Type 1 mode with a pinned contact line and an axisymmetric mode of oscillation, and type 2 with a mobile, circular contact line but an oscillating radius. They also derived a model for finding the resonance frequency of a drop subjected to an acceleration at a frequency f as follows:

$$a = -(2\pi f)^2 u_o \cos(2\pi f t) \tag{1.6}$$

where u_o is the spatial displacement of the substrate. The resonant angular velocity is given by:

$$\omega_j^2 = \left(g q_j + \frac{\gamma}{\rho} q_j^3\right) \tanh\left(q_j \frac{V}{\pi R^2}\right) \tag{1.7}$$

where *g* is acceleration due to gravity, q_j is pseudo wave vector value, *γ* is surface tension between liquid and vapor, *ρ* is the density of the liquid, *V* is the volume of the drop and *R* is the radius of the drop. q_j is defined as

$$q_j = \frac{\pi(j - 0.5)}{p} \tag{1.8}$$

Here *p* is the half arc length of the droplet and is calculated experimentally. Boreyko *et al.* [30] came up with an expression for *p* as follows:

$$p = R\theta \tag{1.9}$$

Quéré [31] suggested that the droplet radius can be calculated based on contact angle and droplet volume as

$$R = \left(\frac{3V}{\pi(1 - \cos\theta)^2 (2 + \cos\theta)}\right)^{\frac{1}{3}} \tag{1.10}$$

Lamb [32] developed an expression for different vibration modes of a free liquid drop, neglecting the viscous damping in the drop.

$$\omega = \sqrt{\frac{\gamma}{3\pi m} l(l-1)(l+2)} \tag{1.11}$$

where ω is the resonant frequency, *l* is an integer value of 2 or higher, γ and *m* are the surface tension and mass of the drop, respectively.

Strani and Sabetta [33] analyzed axisymmetric free vibrations of a drop inside an outer fluid which is in partial contact with a surface. They found out the existence of an additional vibration mode which becomes a zero-frequency rigid mode as the contact

area tends to zero. They also found that adding a solid support increases the resonance frequency of a drop when compared to the corresponding Rayleigh modes.

1.5 Effects of lateral vibration on droplets

While there are several studies available for drops undergoing longitudinal vibrations, studies for drops undergoing lateral vibrations are very few.

Dong *et al.* [34] simulated various modes of a droplet undergoing horizontal vibrations using the Volume of Fluid (VOF) approach in ANSYS Fluent. They compared the various modes identified from the simulations with experimental data. Their findings are shown in the Fig. 1.9 below.

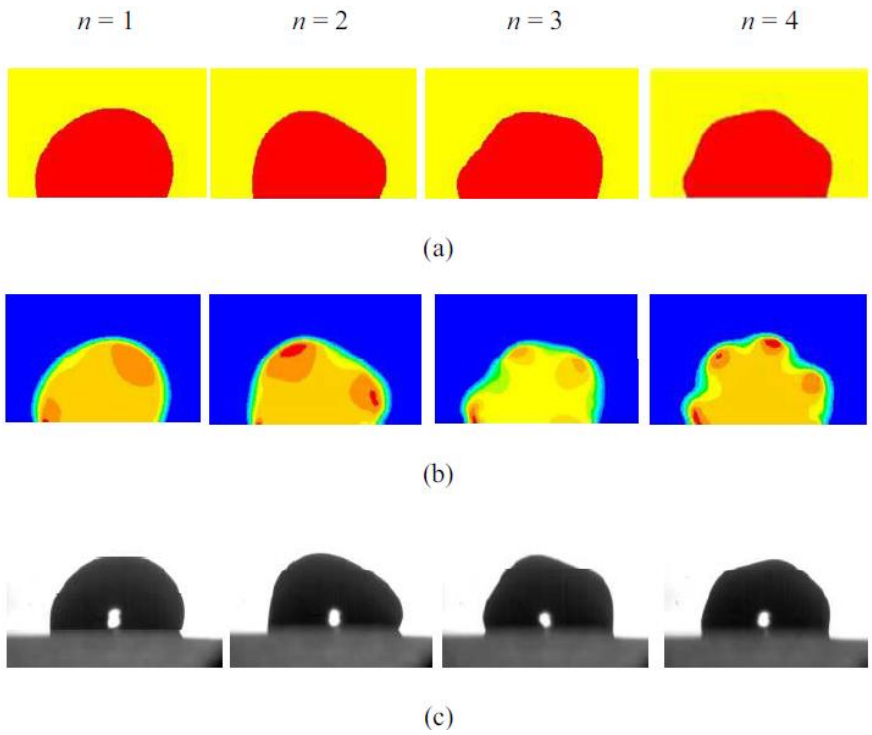

Figure 1.9: First four resonance modes of a vibrating water drop: (a) simulated images, (b) pressure contours, and (c) experimental images. Reprinted from [34]

The first mode corresponds to the rocking mode, where the contact line of the droplet does not slip or move. The droplet oscillates without any downward velocity when placed on a vertical surface. However, when the acceleration is gradually increased, the rocking motion transforms into ratcheting motion. In this motion, the contact line slips and the droplet has a net downward velocity, while ratcheting back and forth the entire way [35]. In the second, third and fourth modes, there are crests appearing on the surface of the drops depending on the resonant mode [34].

In Dong *et. al.'s* [34] CFD simulation were performed for a droplet on a vertical vibrating surface. Fig. 1.10 below shows the horizontal-velocity profile of a drop on a vertically vibrating surface. The simulations were carried out with a droplet volume of 2 μl, vibration frequency of 90 Hz, amplitude of 0.12 mm and a contact angle of 97^{o}. They observed three distinct regions in the velocity profile. Closest to the substrate is the Stokes layer, where the fluid has a very large velocity gradient due to substrate momentum transfer. In the sublinear velocity gradient region, the drop performs a swinging oscillation like a spring pivoted at one end. In the free-surface region, capillary waves develop on the free surface, causing the velocity profile to oscillate. It was observed that gravity enhanced the first resonant mode and weakened the second mode. These phenomena are especially useful in our current work of using vertical vibrations to induce droplet shedding.

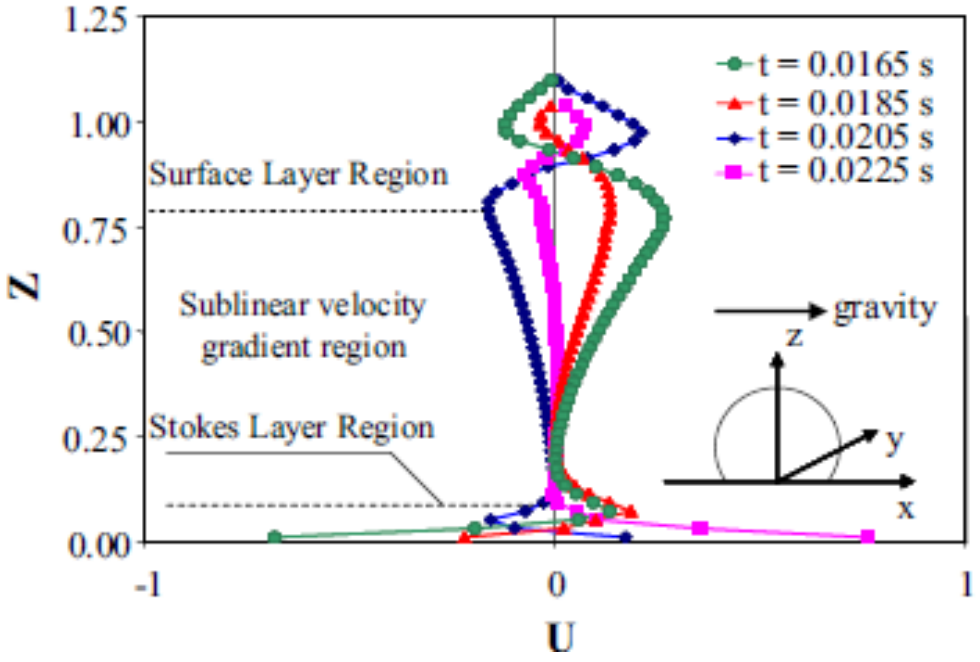

Figure 1.10: Velocity profile for a droplet vibrating on a vertical surface. Reprinted from [34]

Daniel *et al.* [36, 37] did one of the first few works in studying the motion of liquid droplets due to wettability gradient in the presence of contact angle hysteresis. While droplets have a natural tendency to migrate towards the region of higher wettability, they have to be large enough to accomplish that. For a droplet to move, the applied force – like gravity or wettability gradient – must overcome the surface tension effects represented or accounted for by contact angle hysteresis.

To aid the movement of droplets, the authors [36, 37] subjected the horizontal surfaces with an in-plane vibration using a square wave function. They observed that the droplets which otherwise were stuck due to contact angle hysteresis, started moving when vibrated. Similarly, the larger droplets which did move before, moved even faster

when vibrated. Vibrations are most effective when applied to droplets with large contact angle hysteresis. The authors later used the findings to develop a drop propulsion technique by making use of axisymmetric vibrations. [37]

Huber *et al.* [35] applied vibrations in both x and y directions simultaneously. Through simulations and experiments, they found out that rocking and ratcheting motion was seen due to forces only in the y direction, while a combination of x and y direction vibrations led to ejection. They also proved that the transition from rocking to ratcheting motion (in other words, sliding) is a function of acceleration for droplet with the same mass, and independent of amplitude or frequency of vibrations.

Celestini *et al.* [38] derived an expression for finding out the first eigen-frequency of a droplet on a substrate undergoing lateral vibrations. They used a simple oscillator model to find out the corresponding eigen-frequency as follows:

$$\omega_o = \sqrt{\frac{6\gamma h(\theta)}{\rho(1-\cos\theta)(2+\cos\theta)}} R^{-\frac{3}{2}} \qquad (1.12)$$

Here ρ is the liquid density, γ is the surface tension between liquid and vapor and R is the drop radius. h (θ) is numerically computed and is based on droplet deformation due to surface energy minimization caused by an external force. h (θ) is material independent and can be used for different systems, as shown in Fig.1.11.

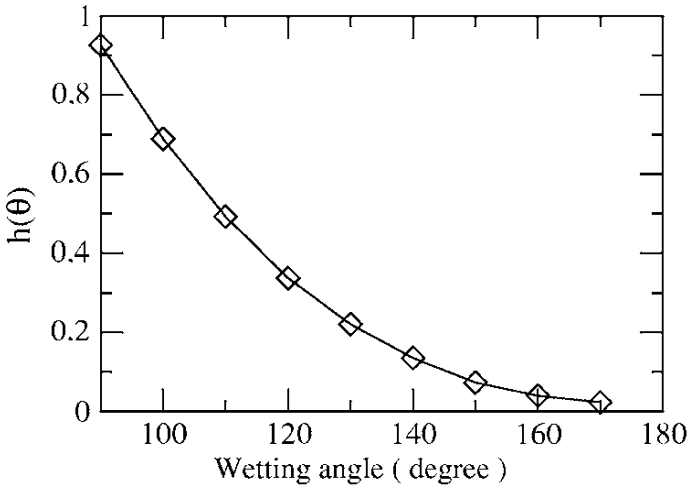

Figure 1.11: h (θ), a numerically computed parameter. Reprinted from [38]

When a droplet is vibrated through the movement of a substrate, the substrate momentum is transferred within the liquid over a distance, called the Stokes length, which is given by:

$$\delta = \sqrt{\frac{2\mu}{\omega}} \tag{1.13}$$

where μ is the kinematic viscosity.

The authors also proposed a first order correction and defined an effective equilibrium contact angle θ_{eff}. While Stokes length is small compared to droplet radius, the effective contact angle is given by:

$$\theta_{eff} = \theta - \frac{\delta}{R \sin\theta} \tag{1.14}$$

The corrected eigen value frequency can be calculated by substituting θ by θ_{eff} in Equation 1.10. The authors found good agreement (up to 15% difference) between

calculated and experimental resonance frequencies for droplets of mercury vibrated on glass slides.

Thus, from the above discussion, it is evident that vibrations could be useful in increasing condensation heat transfer due to faster droplet sliding. Also, vibrations imposed at resonance frequencies may cause droplets to move significantly. However, there have been limited experimental data for droplet sliding under the effects of resonant frequencies on both hydrophilic and hydrophobic surfaces.

1.6 Concluding remarks

Vibrations should be used to promote droplet sliding which could in turn enhance DWC through effective droplet shedding. As pointed out above, there have been several studies and proposed models used to determine resonance in vibrating droplets. The effects of resonance on droplets are known to a certain extent, but the effect of vibration on droplet shedding in DWC still is unknown. This study focuses on the effectiveness of resonant frequencies on droplet sliding. It is also important to understand the effects of resonant frequencies on droplet sitting on hydrophobic surfaces.

In summary, the objectives of this study include experimentally determining the resonant frequencies of submilliliter droplets on different surfaces. The study also focuses on the role of acceleration and amplitude in droplet sliding on vertical surfaces. Finally, the effects of imposing resonant vibrations on droplet sliding are also investigated.

2. EXPERIMENTAL SETUP AND PROCEDURE

The objectives of the study are to understand the role of vibration parameters such as resonant frequencies of droplets on sliding. Specifically, the effects of resonant frequencies of droplets sitting on hydrophilic and hydrophobic surfaces, as well as vibration acceleration should be investigated.

2.1 Overall setup

To meet the goals of the study, an experimental set-up was designed as shown below. The setup consisted of a speaker, amplifier, high speed camera, data acquisition system, vibration sensor, backlight illumination, computer, stand for affixing surfaces to, and a tilting mechanism for the speaker.

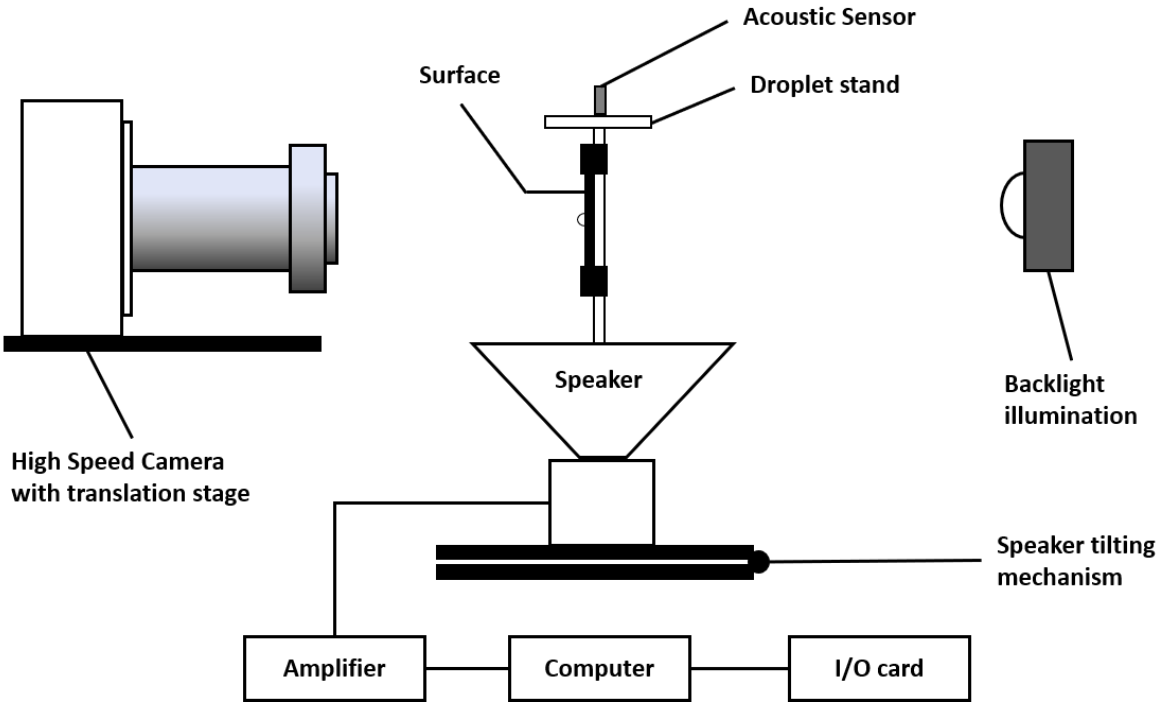

Figure 2.1: Schematic of the overall setup

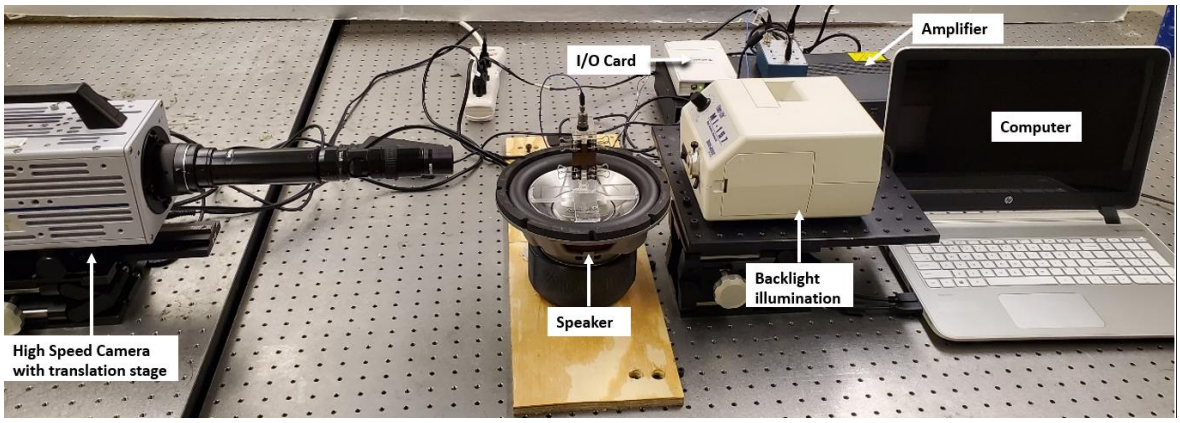

Figure 2.2: Photograph of the overall setup

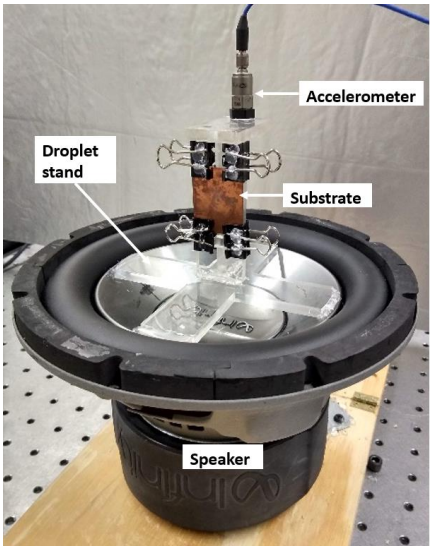

Figure 2.3: Vibration system

All the experiments were performed on a pneumatically damped optical table to avoid any ambient noise. The temperature for the experiments was about 21-22^{o} C. The other components of the system are described below.

2.1.1 Substrates

Three substrates with increasing levels of wettability were used in this study, each measuring 28 mm x 35 mm (1-1/8” x 1-3/8”). Copper substrates were cut from a 1.6 mm (1/16”) thick sheet of Copper supplied by Grainger. Polytetrafluoroethylene (PTFE) substrates were cut from a 3.2 mm (1/8”) thick sheet of PTFE supplied by McMaster-Carr. The third substrate was developed by spraying four coats of ‘Saphir Medaille d’Or Super Invulner – Waterproof Spray’ on PTFE surfaces, with each coat dried for an hour before the next one was applied. This sample will henceforth be referred to in this study as ‘Saphir’.

The roughness of these substrates was measured using a profilometer (Profilm3D, Filmetrics Inc).

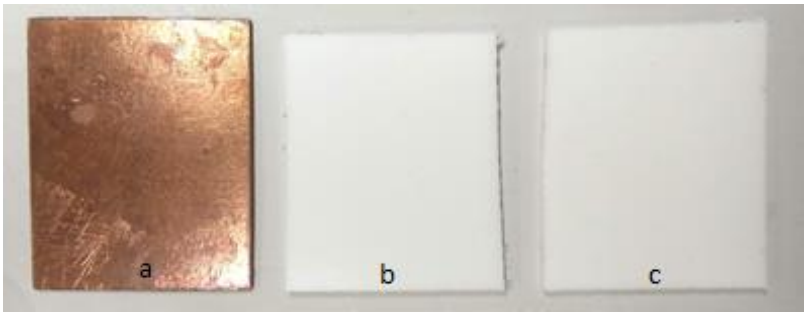

Figure 2.4: Test Specimens used: a) Copper b) PTFE c) Saphir

2.1.2 Droplet stand

A droplet stand was used to affix the substrates to the speaker. All the parts of this assembly have an interlocking mechanism to make sure that the considered angles were precise. The stand was affixed to the woofer of the speaker using a level. The stand allows for vertical and lateral droplet vibration testing. There was also space at the top to affix the vibration sensor.

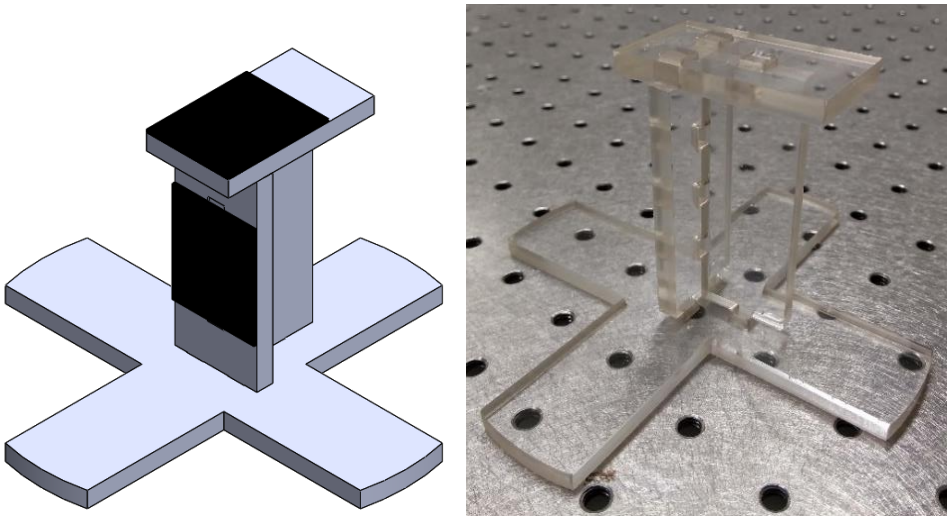

Figure 2.5: Droplet stand

2.1.3 Vibrational system

A sound speaker (Infinity Reference 860 W, Infinity Inc.) was used to provide the vertical vibrations to the droplet stand. The speaker was connected to an amplifier system (Russound P75-2 Channel Dual Source 75 W). The frequency response of the speaker was adjusted from 20 Hz to 200 Hz for all vibration experiments. An online tone generator [39] was used to generate the frequencies from the speaker.

Figure 2.6: Sound speaker (Infinity Reference 860 W, Infinity Inc.)

2.1.4 Data acquisition system

An accelerometer (352C04, PCB Piezoelectronics) was connected to an accelerometer power supply (P5000, MISTRAS) to measure vibration frequencies and accelerations emanating from the test substrate. A data acquisition system (NI USB-5132, National Instruments, Inc.) was used to interface the accelerometer with the computer. The signals from the sensor were collected and analyzed from NI (National Instruments) Scope and outputs for voltage, frequency and intensity were obtained. The sensor had a sensitivity of 10 mV/g, measurement range of ±500 g, frequency range of 0.5 – 10000 Hz (± 5%) and a resolution of 0.0005 g (rms).

Figure 2.7: Accelerometer (352C04, PCB Piezoelectronics)

2.1.5 Imaging system

A high-speed camera (Photron SA3) was used to record the static and dynamic images of the droplets. The camera was placed on a translation stage to aid with focusing. The camera can record up to 60,000 frames per second and with a resolution of 1024 x 1024.

Figure 2.8: High speed camera (Photron SA3)

2.1.6 Backlight illumination

A Halogen light source (Fiber-Lite MI series, Dolan-Jenner Inc.) was used for enabling the high-speed camera to capture high contrast sharp images. To achieve high level of brightness over a lesser area, a light focusing attachment was used at the outlet of the light source.

Figure 2.9: Halogen light source (Fiber-Lite MI series, Dolan-Jenner Inc.)

2.2 Contact angle measurement technique

To determine the contact angle of water droplets on different substrates, droplets of different sizes ranging from 3.8 – 6.8 μl were deposited on a horizontal test specimen using a micropipette. The micropipette was calibrated using a weight scale with a resolution of 0.1 mg considering the density of water. Images of droplets sitting on the substrates were captured using the high-speed camera. The contact angle of each droplet,

under static conditions on horizontal substrate, as well as on vertical substrate was measured using 'Drop Shape Analysis' plug-in [40] of ImageJ software. The process involves placing 7 to 10 points along the perimeter of the drop to determine the contact angle. Figure 2.10 below shows an example how droplet contact angle on a substrate was determined.

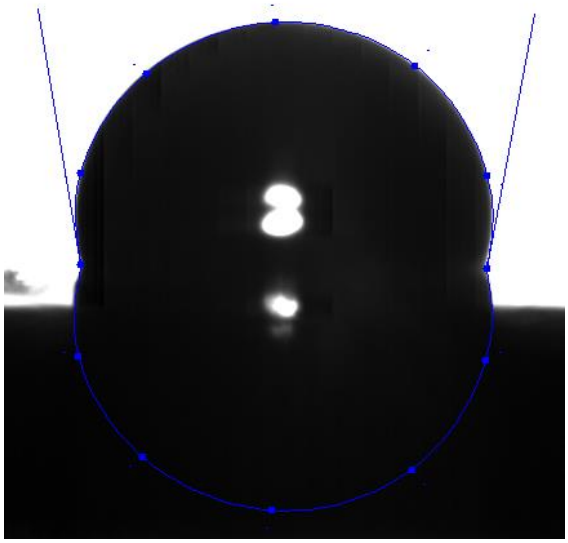

Figure 2.10: Contact angle on each side of the droplet are 100.3^{o} and 100.0^{o} for a 4.8 μl droplet on a horizontal PTFE substrate

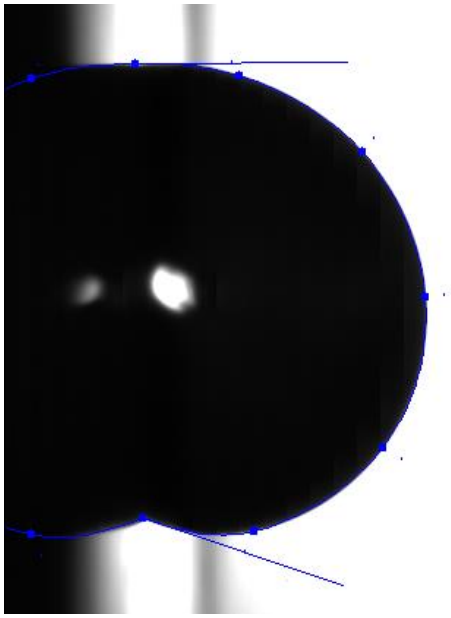

Figure 2.11: Advancing and receding contact angle are 89.6^{o} and 109.4^{o} for a 4.8 μl droplet on a vertical PTFE substrate

2.3 Resonant frequency measurement and identification technique

Several techniques have been suggested in the literature to determine the resonant frequency of vibrating droplets. Some of the commonly used techniques involve vibrating droplets at constant amplitude and increasing frequencies, and required making the following observations:

a) Deformation [38]

b) Contact angle hysteresis [38]

c) Motion of center of the mass [33]

In the current study, contact angle hysteresis was used to identify resonant frequencies. The technique is quite applicable when using both hydrophilic and hydrophobic substrates.

To determine the resonant frequency, the Celestini's model (Equation 1.12) was used to estimate the corresponding resonant frequency by using droplet volume, and static contact angle as input variables. Experiments were started at the predicted frequency and increased in increments of 5 Hz. The high-speed camera was used at 1000 frames per second during the experiments. For each of the tested frequencies, outlines of 200 frames (0.2 s) were superimposed on each other. The outlines were generated using the Canny algorithm of MATLAB with a threshold of 0.1.

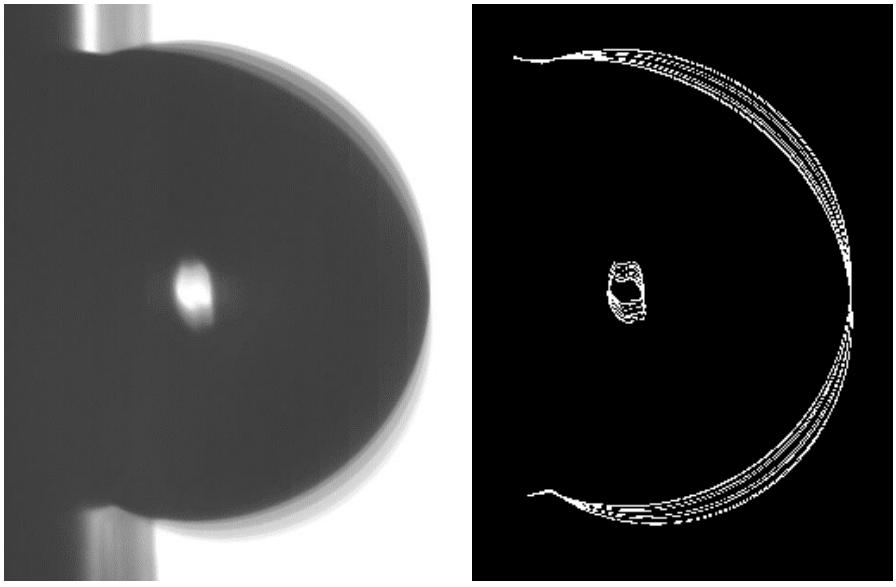

Figure 2.12: Superimposition of images (left) and outlines (right) of a 3.8 μl vibrating droplet on PTFE

From the superimposition of outlines, the outline with the maximum lateral displacement was identified and used to determine contact angle hysteresis of the droplet as shown in Fig. 2.13.

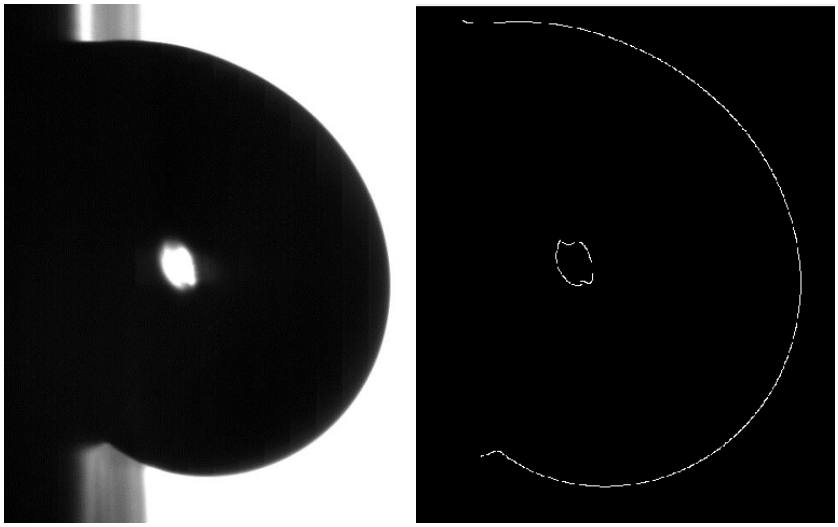

Figure 2.13: Droplet position with maximum CAH (PTFE, 3.8 μl). Actual image on the left and outline on the right

Contact angle hysteresis was calculated using Drop Shape Analysis plugin of ImageJ software as shown in Fig. 2.14.

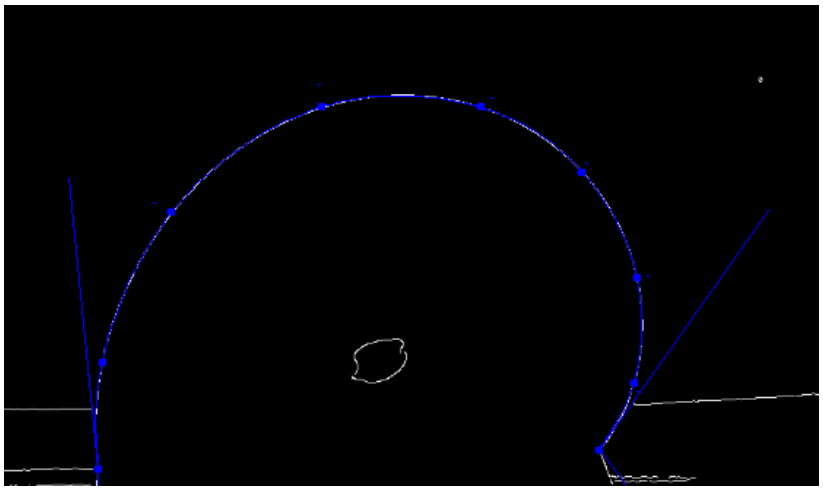

Figure 2.14: Advancing and receding contact angle are 93.4° and 127.7° for a 3.8 μl droplet on a vertical PTFE substrate

Maximum contact Angle hysteresis for different frequencies was noted at the same amplitude of vibration. Once an estimate of the resonant frequency was found, the input frequency was increased in increments of 1 Hz. The frequency with the maximum CAH was deemed or considered to be the resonant frequency of the droplet.

2.4 Determination of sliding parameters

One of the goals of the study was to identify the values of the different vibration parameters that had an effect on droplet sliding. Among the vibration parameters, frequency, acceleration, and amplitude were measured and calculated for each test. Initially the substrate was vibrated at the identified resonant frequency of the droplet at low amplitude or acceleration. High speed images were captured every second to identify the onset of sliding. Outlines of the frames were superimposed to observe any shift of the

droplet outline, which was used to identify the moment of droplet sliding. If no sliding was observed, then the amplitude of vibration was increased until the droplet began to slide.

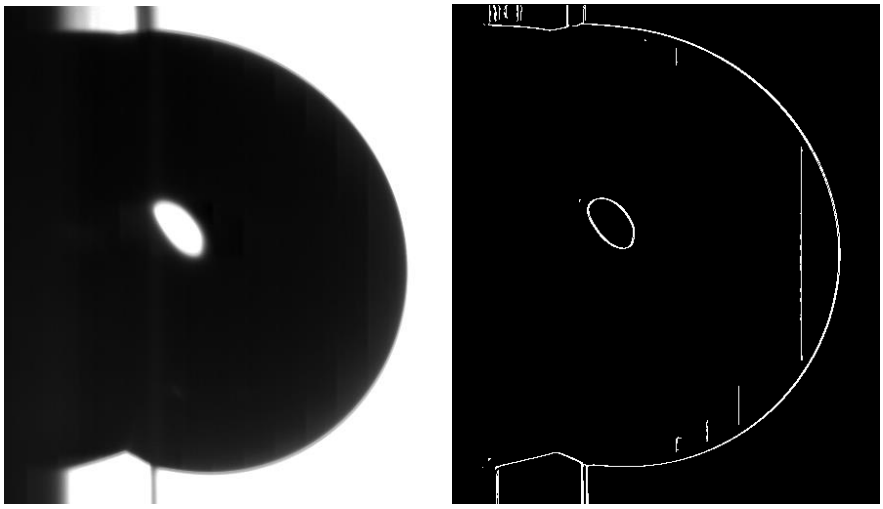

Figure 2.15: No sliding observed on a 3.8 μl droplet on PTFE with .an acceleration of 0.5g

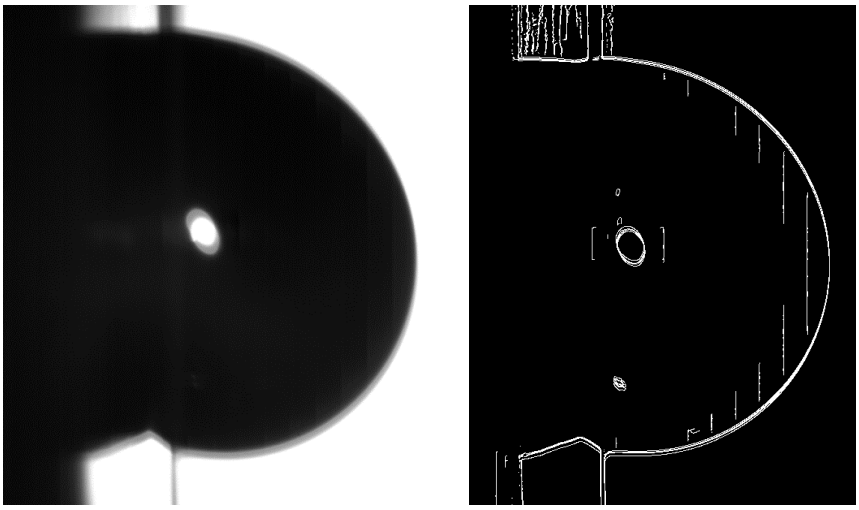

Figure 2.16: Fully developed sliding behavior observed on a 3.8 μl droplet on PTFE with an acceleration of 0.8 g

The sliding experiments were repeated at frequencies ±25 % and ±50 % of the corresponding resonant frequency. Amplitude, acceleration and vibration intensity of the sample were measured during the droplet sliding events.

2.5 Experimental plan and conditions

In this study, different substrates and water droplet volumes were considered for the vibration experiments, as follows:

1. Copper: Copper has a very high thermal conductivity. Combined with its easy workability, it is an excellent material to manufacture heat transfer coils.
2. PTFE: PTFE is one of the most hydrophobic plastics available. Its low cost and friction coefficient make it suitable for droplet sliding.
3. Saphir: Saphir was manufactured in the lab as a material more hydrophobic than PTFE. It is also rougher than PTFE which is discussed in the next chapter.

In addition to the different substrates used during the experiments, different droplet sizes were considered, as shown in Table 2.1.

Droplet size such as 3.3 μl, 5.8 μl and 6.8 μl were also used to determine resonant frequencies. The droplet sizes shown in Table 2.1 are representative of droplet sizes observed in dropwise condensation [41-43]. Moreover, droplets smaller than 3.3 μl were difficult to observe and control during experiments.

The following experimental variables were measured or calculated:

1. Amplitude (calculated): Amplitude of vibration is an important variable in the design the vibrating substrates.

2. Acceleration (measured): Acceleration of vibration is important so that the vibration intensity and amplitude could be determined.
3. Vibration intensity (calculated): Vibration intensity, defined as the product of amplitude and frequency, is important to characterize the vibrations incident on the droplet completely.

In total, 9 cases were considered for the sliding experiments, which include the use of three substrates and at least three droplet volumes. The results are discussed in the following chapter.

Table 2.1: Experimental independent variables

Substrate Type	Droplet Volume, μl
Copper	3.8, 4.3, 4.8, 5.8, 6.8
PTFE	3.3, 3.6, 3.8, 4.0, 4.3, 4.8, 5.8
Saphir	3.3, 3.8, 4.3, 4.8

3. RESULTS AND DISCUSSION

In this chapter, droplet characteristics on different substrates based on theoretical and experimental results are presented. First, the resonant frequencies due to lateral vibrations of droplets on substrates of varying wettability are presented. The experimental and theoretical frequencies are compared as well. Then, the effects of varying amplitude and frequency of vibrations on droplets, especially during droplet sliding is investigated. Finally, the effects of imposing resonant vibrations are determined and quantified.

3.1 Substrate characterization

As mentioned in the previous chapter, three substrates were used in the study, namely Copper, PTFE and Saphir. Firstly, the roughness of the substrates were measured using a profilometer. The images captured during the process for copper, PTFE and Saphir are shown in Fig. 3.1, 3.2 and 3.3 respectively.

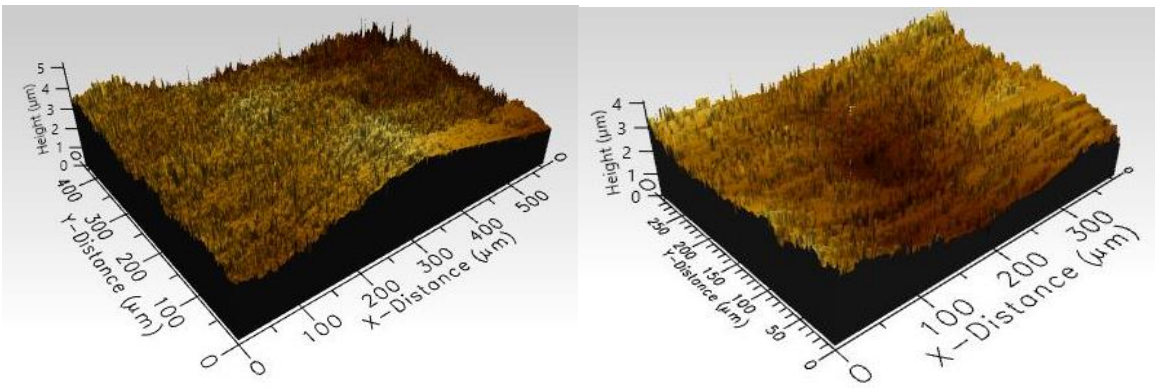

Figure 3.1: Roughness profile of copper substrate

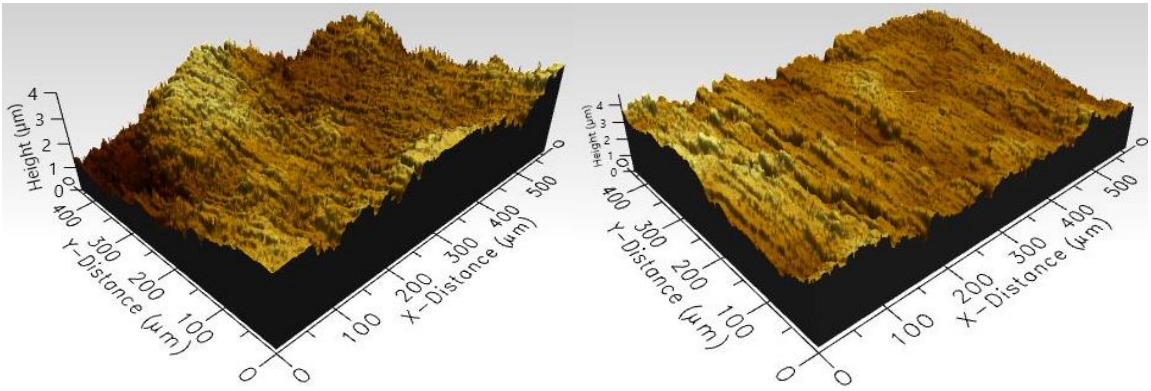

Figure 3.2: Roughness profile of PTFE substrate

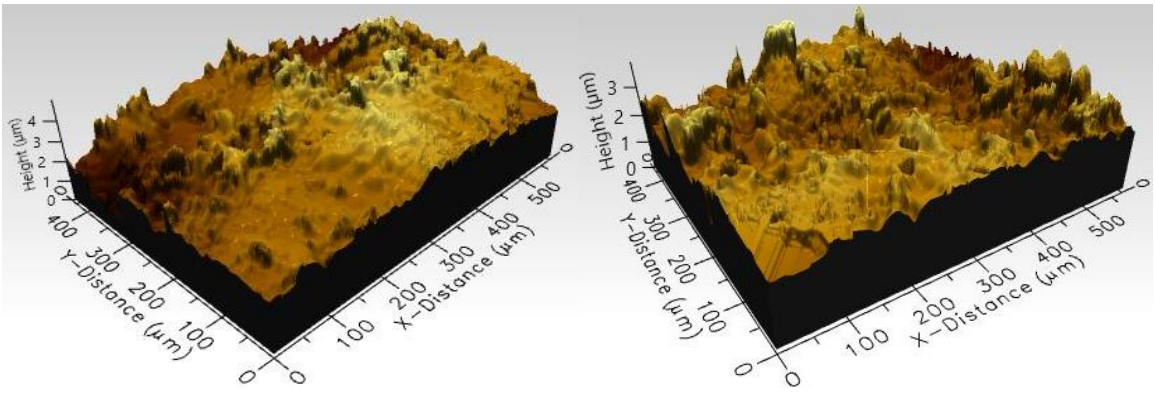

Figure 3.3: Roughness profile of Saphir substrate

As shown in the figures above, commercially available copper is relatively rougher in nature than PTFE. Furthermore, Saphir, which was produced by spray coating on PTFE, led to higher average roughness value and greater roughness variation as seen in Table 3.1.

Table 3.1: Average and standard deviation of roughness for the substrates

Substrate	Average Roughness (μm)	Roughness Standard Deviation (μm)
Copper	0.62	0.082
PTFE	0.37	0.047
Saphir	0.44	0.090

The static contact angle of droplets on these substrates was measured by imaging each droplet at rest on a horizontal substrate. For the advancing and receding contact angles, each droplet was placed on a substrate horizontally, then the substrate was tilted. Drop Shape Analysis plugin of ImageJ was used for analysis. Results are shown in Table 3.2.

Table 3.2: Static contact angles of droplets on different substrates

Substrate	Static Contact Angle	Advancing Contact Angle	Receding Contact Angle	Contact Angle Hysteresis
Copper	85.5°	94.9°	75.2°	19.7°
PTFE	100.0°	110.5°	90.7°	19.8°
Saphir	115.9°	100.6°	124.3°	23.7°

3.2 Micropipette calibration

Each droplet weight dispensed by the micropipette was determined using a precision balance (APEX Series, Denver Instrument). Each weight was converted to droplet volumes using a density value of 997 kg/m^3. The measured droplet volume vs. dispensed droplet volume are shown in Fig. 3.4.

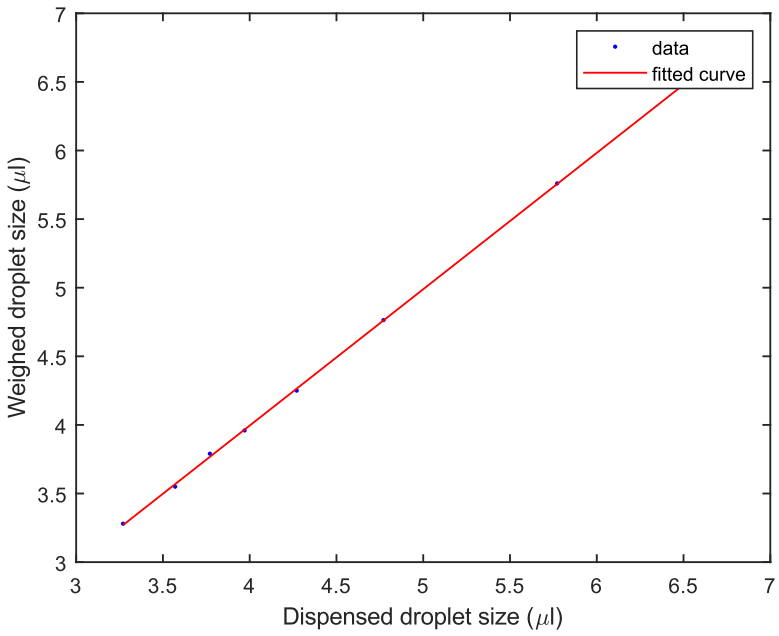

Figure 3.4: Weighted droplet volume vs. dispensed droplet volume

The R^2 value of the plot above is 0.999, which assures linearity of the weighted and dispensed droplet volume. Thus, the accuracy of the micropipette has been verified.

3.3 Droplet size determination

To compare the droplet volume given by Equation 1.10 shown in Section 1.5 with the experimentally measured droplet volume, the radius of each droplet deposited on a horizontal substrate was measured. A wire of known diameter (1.825 mm) was used for visual calibration. The results are shown in Table 3.2.

Table 3.3: Comparison between experimental and theoretical droplet radius

Material	Droplet Size (μl)	Experimental Droplet Radius (mm)	Theoretical Droplet Radius, Eq. 10 (mm)	% Difference
Copper	6.8	1.51	1.54	1.5
	5.8	1.47	1.46	1.0
	4.8	1.35	1.37	1.3
	4.3	1.32	1.32	0.2
	3.8	1.28	1.26	1.1
PTFE	5.8	1.27	1.30	2.5
	4.8	1.20	1.22	1.8
	4.3	1.16	1.17	1.5
	4.0	1.10	1.15	4.3
	3.8	1.06	1.13	6.1
	3.6	1.04	1.11	6.1
	3.3	1.02	1.07	4.9

Table 3.3 Continued

Material	Droplet Size (μl)	Experimental Droplet Radius (mm)	Theoretical Droplet Radius, Eq. 10 (mm)	% Difference
Saphir	4.8	1.12	1.12	0.3
	4.3	1.06	1.08	1.8
	3.8	1.03	1.04	1.0
	3.3	0.99	0.99	0.2

The average difference between the calculated and measured droplet radii was less than 2.2%. Therefore, using Equation 1.10 for estimating droplet radii based on static contact angle and droplet volume was found to be acceptable.

3.4 Resonant frequency of droplets

This section includes the results of resonant frequencies of droplets obtained from Celestini's model described in Section 1.5 and experiments and discusses the difference between the calculated and experimental values.

3.4.1 Calculated resonant frequency

The theoretical resonant frequency for first (rocking) mode was calculated from the Celestini's model described in Section 1.5. Acceleration due to gravity (g), surface tension (γ), density of water (ρ) and kinematic viscosity of water (μ) were taken as 9.81 m/s^2, 72.8 mN/m^2, 997 kg/m^3 and 9.783e^{-7} m^2/s respectively. Values for h (θ) were calculated from interpolation using Figure 1.12. A first order correction was made by using Equation 1.14 and substituting θ_{eff} in Equation 1.10. The calculated results are presented in Fig. 3.5.

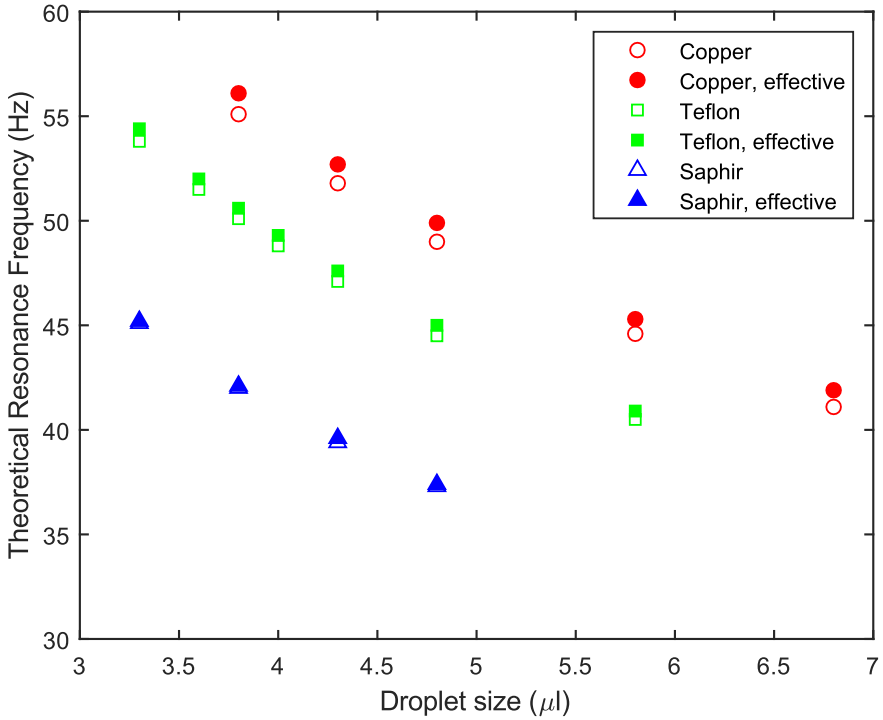

Figure 3.5: Theoretical resonant frequency for different substrates

3.4.2 Experimental resonant frequencies

As mentioned in Section 2.3 of the previous chapter, droplets were vibrated at constant amplitude but at varying frequencies. The frequency corresponding to the maximum contact angle hysteresis was deemed as the resonant frequency of the droplet-substrate pair. For illustration purposes, the resonant frequency of a droplet of size 4.8 μl was used in all of the three substrates considered in the study, as shown in Fig 3.6, 3.8 and 3.10.

For Copper, the vibration experiments were started at a frequency of 55 Hz and continued in increments of 5 Hz till 70 Hz. Once a rough estimate of the resonant frequency

was found, the experiments were repeated in increments of 1 Hz until the resonant frequency was eventually identified. Fig. 3.6 shows a 4.8 μl droplet vibrating on a copper substrate at resonance.

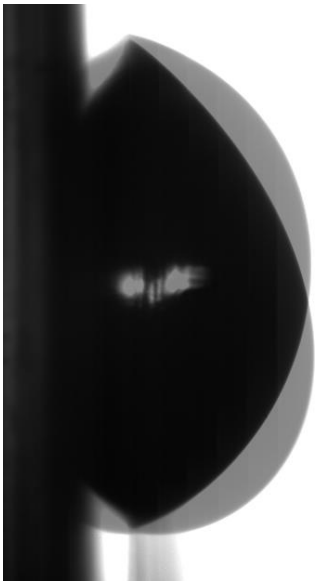

Figure 3.6: Motion of a 4.8 μl droplet on copper at resonance (58 Hz)

Fig. 3.7. shows experimental contact angle hysteresis as a function of imposed vibrating frequency. As the figure shows, at a particular frequency, the droplet experiences maximum contact angle hysteresis, which corresponds to the resonance condition.

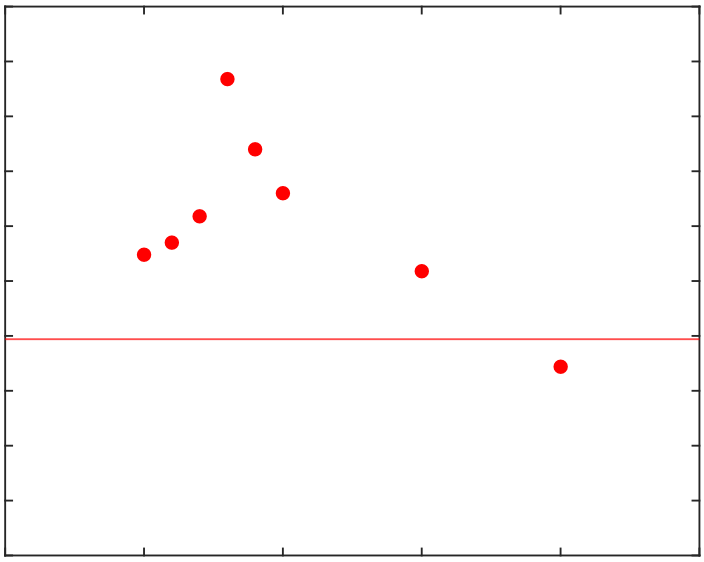

Figure 3.7: Contact angle hysteresis as a function of frequency for a 4.8 μl droplet on copper without droplet sliding

For PTFE, the experiments were started at a vibrating frequency 50 Hz and continued in increments of 5 Hz till 60 Hz. After getting a rough estimate of the resonant frequency, the experiments were repeated in increments of 1 Hz until the resonant frequency was identified. Fig. 3.8 shows a 4.8 μl vibrating on a PTFE substrate at resonance.

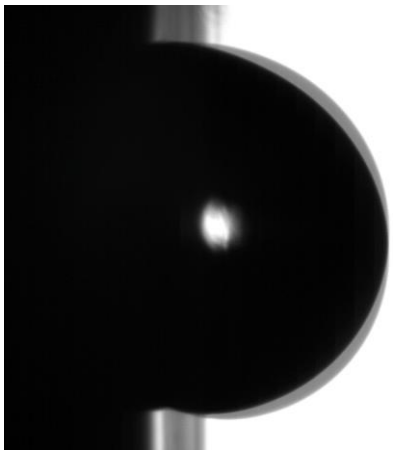

Figure 3.8: Motion of a 4.8 μl droplet on PTFE at resonance (54 Hz)

Fig. 3.9. shows experimental contact angle hysteresis as a function of imposed vibrating frequency. As the figure shows, at a particular frequency, the droplet experiences maximum contact angle hysteresis, which corresponds to the resonance condition.

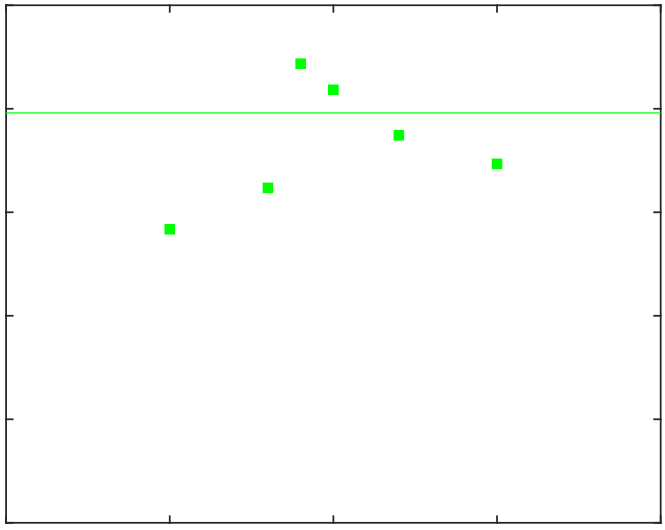

Figure 3.9: Contact angle hysteresis as a function of frequency for a 4.8 μl droplet on PTFE without droplet sliding

For Saphir, the experiments were started at a vibrating frequency of 40 Hz and continued in increments of 5 Hz till 50 Hz. For getting the actual experimental resonant frequency, the experiments were repeated in increments of 1 Hz until the resonant frequency was found. Fig. 3.10 shows a 4.8 μl vibrating on a Saphir substrate at resonance.

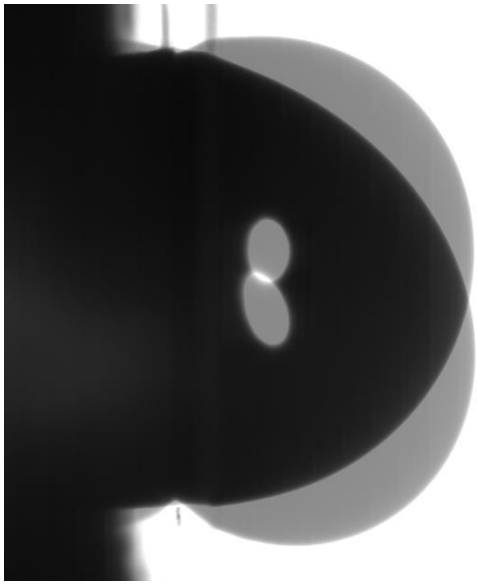

Figure 3.10: Motion of a 4.8 μl droplet on Saphir at resonance (46 Hz)

Fig. 3.11. shows experimental contact angle hysteresis as a function of imposed vibrating frequency. As the figure shows, at a particular frequency, the droplet experiences maximum contact angle hysteresis, which corresponds to the resonance condition.

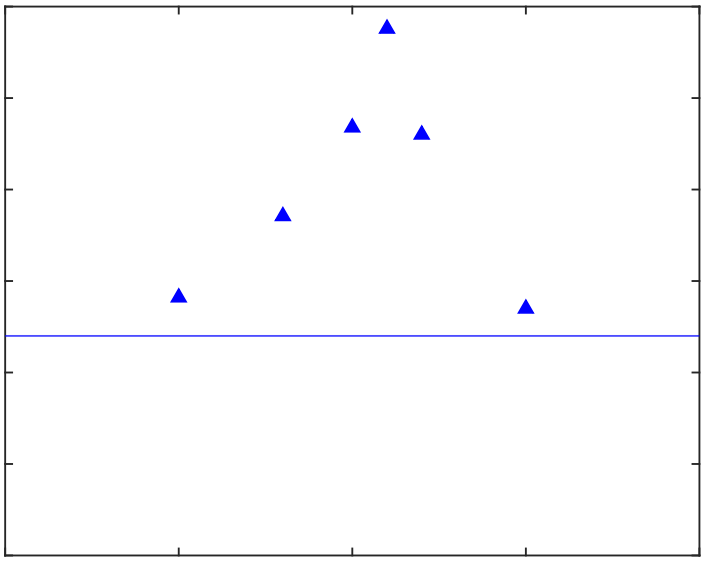

Figure 3.11: Contact angle hysteresis as a function of frequency for a 4.8μl droplet on Saphir without droplet sliding

The summary of the results for all droplet sizes and substrates are presented in Fig. 3.12. From the figure, it can be seen that as hydrophobicity of the substrate increases, the first resonant frequency for the same droplet size decreases. Since a drop on a hydrophobic substrate is more unstable than a drop on a hydrophilic substrate, lesser energy is required for its motion. Furthermore, the energy of vibration is dependent on its frequency, so at resonant frequency less energy is required to induce droplet motion. Moreover, as the figure shows, resonant frequency decreases with droplet volume, which is consistent with previous studies and the Celestini's model. Table 3.3 summarizes all the key results including the resonant frequency and maximum contact angle hysteresis for each droplet-substrate pair.

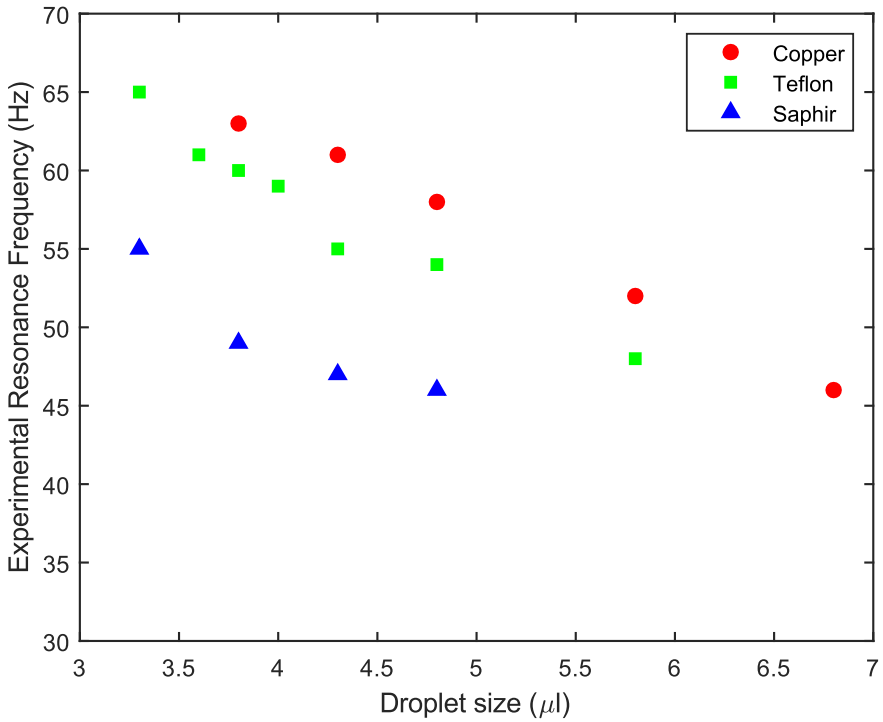

Figure 3.12: Experimental resonant frequency as a function of droplet volume on different substrates

From the above plot, it is seen that across all substrates, as the droplet volume decreases, the resonant frequency increases, which is consistent with the Celestini's model. Furthermore, the resonant frequency of droplet for the same volume decreases with contact angle (i.e. hydrophobicity).

Table 3.4: Experimental resonance frequency and maximum CAH for droplets of varying sizes on different substrates without droplet sliding

Material	Droplet Size (μl)	Experimental Resonant Frequency (Hz)	Static CAH [°]	Maximum CAH [°]
Copper	6.8	46.0	19.7	57.0
	5.8	52.0	19.7	47.7
	4.8	58.0	19.7	43.4
	4.3	61.0	19.7	46.2
	3.8	63.0	19.7	42.3
PTFE	5.8	48.0	19.8	37.9
	4.8	54.0	19.8	20.9
	4.3	55.0	19.8	41.8
	4.0	59.0	19.8	33.2
	3.8	60.0	19.8	31.8
	3.6	61.0	19.8	30.2
	3.3	65.0	19.8	30.3
Saphir	4.8	46.0	23.7	57.6
	4.3	47.0	23.7	62.5
	3.8	49.0	23.7	44.0
	3.3	55.0	23.7	49.7

3.4.3 Comparison of theoretical and experimental resonant frequency

The resonant frequencies from both the model and experiments were compared with each other, as shown in Table 3.4. As the table shows, the effective theoretical frequency always underestimates the actual resonant frequency.

Table 3.5: Summary of experimental and theoretical resonant frequency of droplets

Material	Droplet Size (μl)	Experimental Resonant Frequency (Hz)	Effective Theoretical Frequency (Hz)	Difference (Hz)	% Difference
Copper	6.8	46.0	41.9	4.1	9.9
	5.8	52.0	45.3	6.7	14.7
	4.8	58.0	49.9	8.1	16.3
	4.3	61.0	52.7	8.3	15.7
	3.8	63.0	56.1	6.9	12.3
PTFE	5.8	48.0	40.9	7.1	17.3
	4.8	54.0	45.0	9.0	20.0
	4.3	55.0	47.6	7.4	15.6
	4.0	59.0	49.3	9.7	19.6
	3.8	60.0	50.6	9.4	18.5

Table 3.5 Continued

Material	Droplet Size (μl)	Experimental Resonant Frequency (Hz)	Effective Theoretical Frequency (Hz)	Difference (Hz)	% Difference
PTFE	3.6	61.0	52.0	9.0	17.2
	3.3	65.0	54.4	10.6	19.5
Saphir	4.8	46.0	37.4	8.6	22.9
	4.3	47.0	39.6	7.4	18.8
	3.8	49.0	42.1	6.9	16.3
	3.3	55.0	45.2	9.8	21.6

Figures 3.13 through 3.15 shows the effective theoretical and experimental resonant frequencies for droplets on Copper, PTFE and Saphir substrates, respectively.

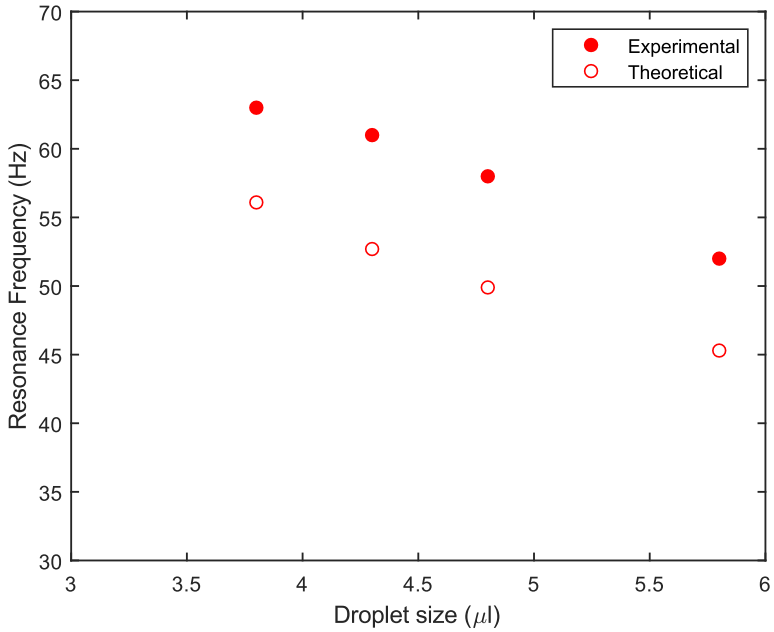

Figure 3.13: Experimental and theoretical resonant frequencies for copper

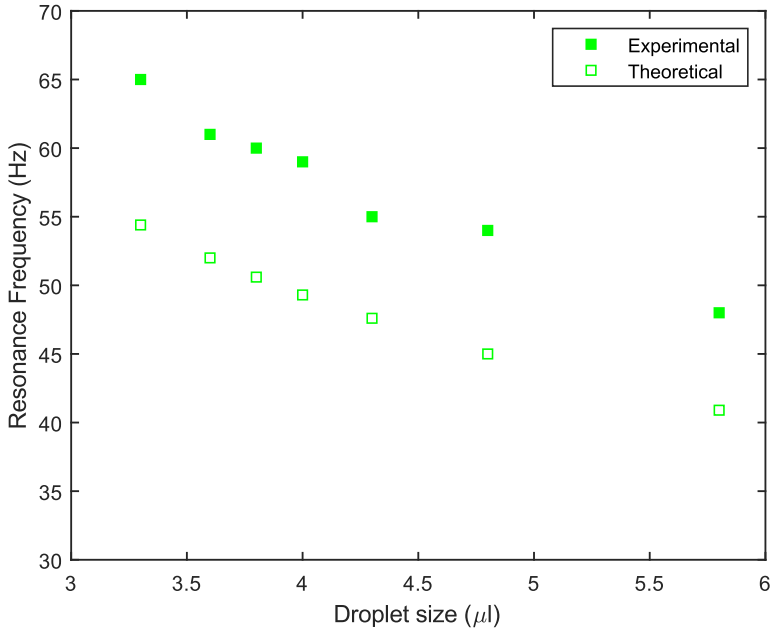

Figure 3.14: Experimental and theoretical resonant frequencies for PTFE

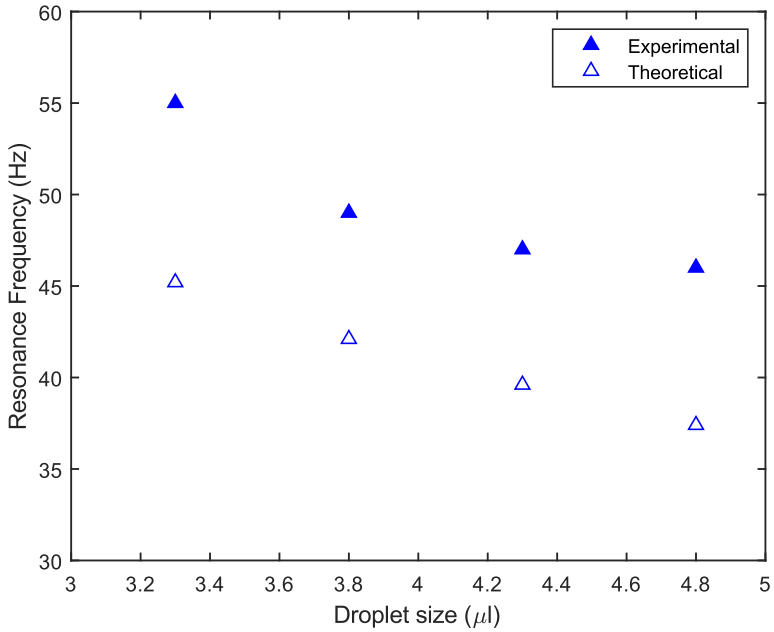

Figure 3.15: Experimental and theoretical resonant frequencies for Saphir

From the above data, the Celestini's model [38] underpredicts the experimental data by about 20 %. A similar trend was observed by Celestini [38] for resonance experiments with drops of mercury on glass slides with a static contact angle of 140^{o}.

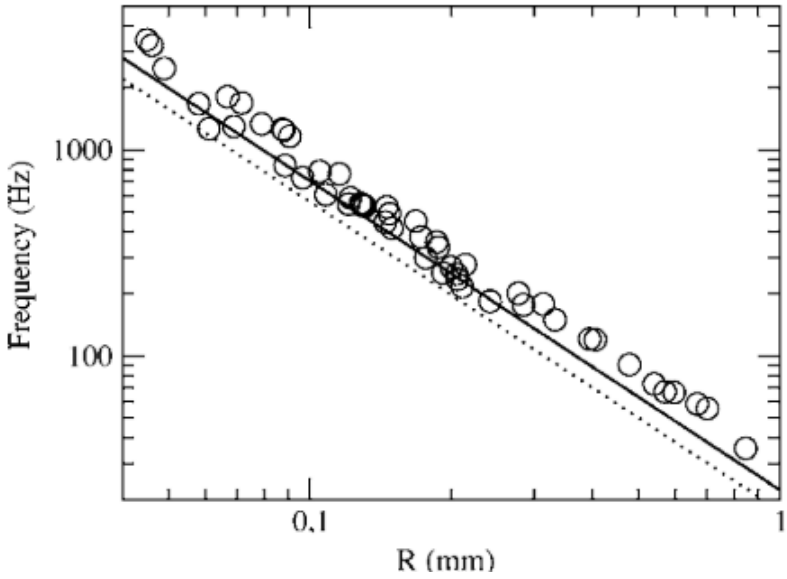

Figure 3.16: Experimental and theoretical resonant frequencies for drops of mercury vibrating on glass slides. Reprinted from [38].

3.5 Sliding of droplets

One of the main objectives of this study is to determine the effect of frequency and acceleration on droplet sliding, and subsequently using resonant frequencies to induce droplet sliding. Once the resonant frequency of a droplet deposited over a substrate was determined, the amplitude of vibrations was increased till sliding was observed, as mentioned in section 2.4.

3.5.1 Effect of droplet size on sliding parameters

The effects of varying droplet sizes on parameters like amplitude, acceleration and vibration intensity during sliding on copper (Fig. 3.17 – 3.19), PTFE (Fig. 3.20 – 3.22) and Saphir (Fig. 3.23 – 3.25) substrates are shown below.

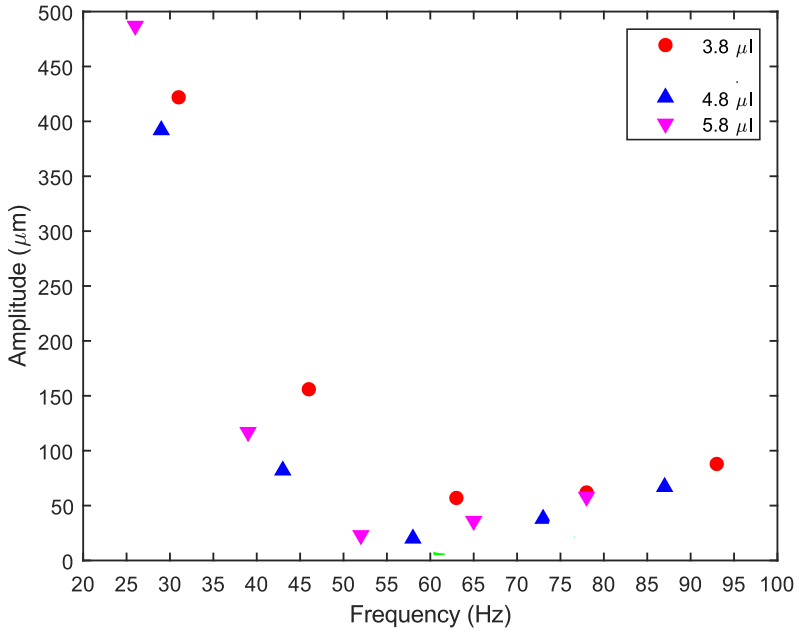

Figure 3.17: Amplitude vs. frequency at sliding for different droplet volumes on copper

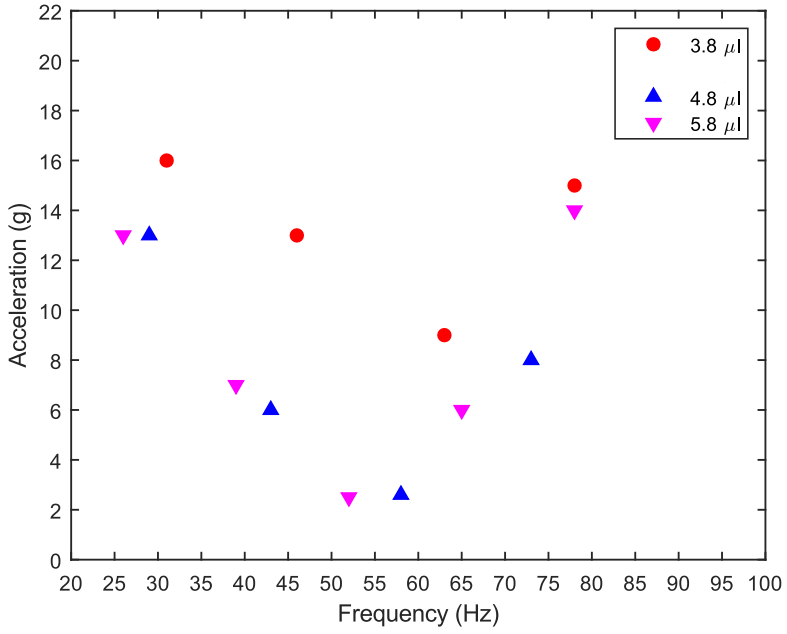

Figure 3.18: Acceleration vs. frequency at sliding for different droplet volumes on copper

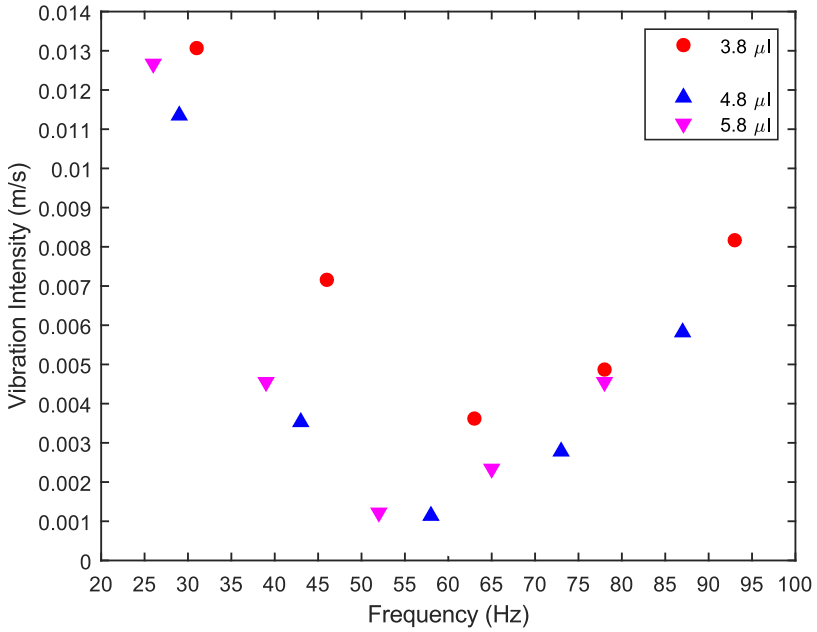

Figure 3.19: Vibration intensity vs. frequency at sliding for different droplet volumes on copper

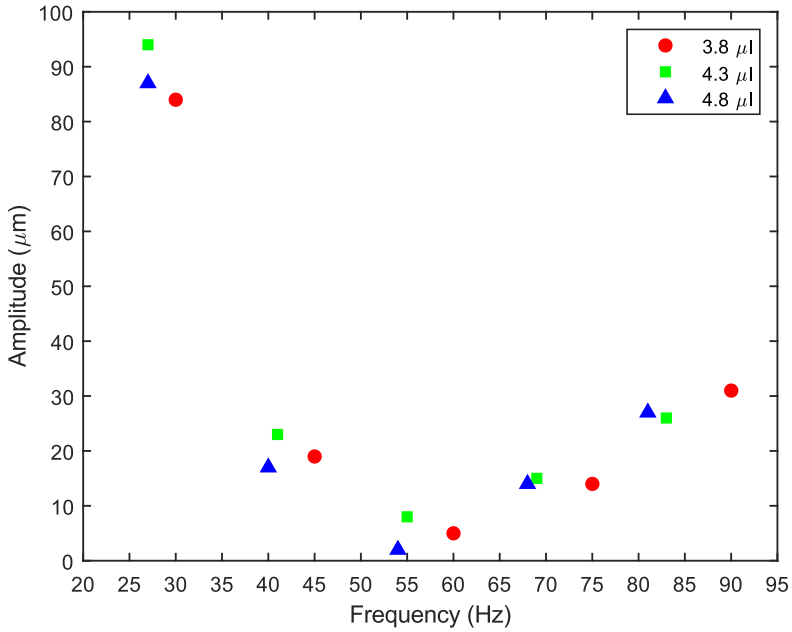

Figure 3.20: Amplitude vs. frequency at sliding for different droplet volumes on PTFE

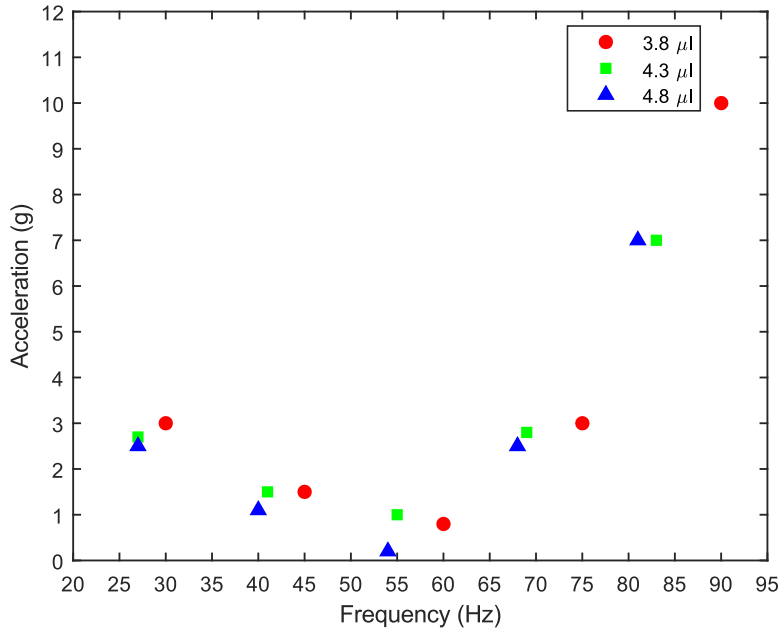

Figure 3.21: Acceleration vs. frequency at sliding for different droplet volumes on PTFE

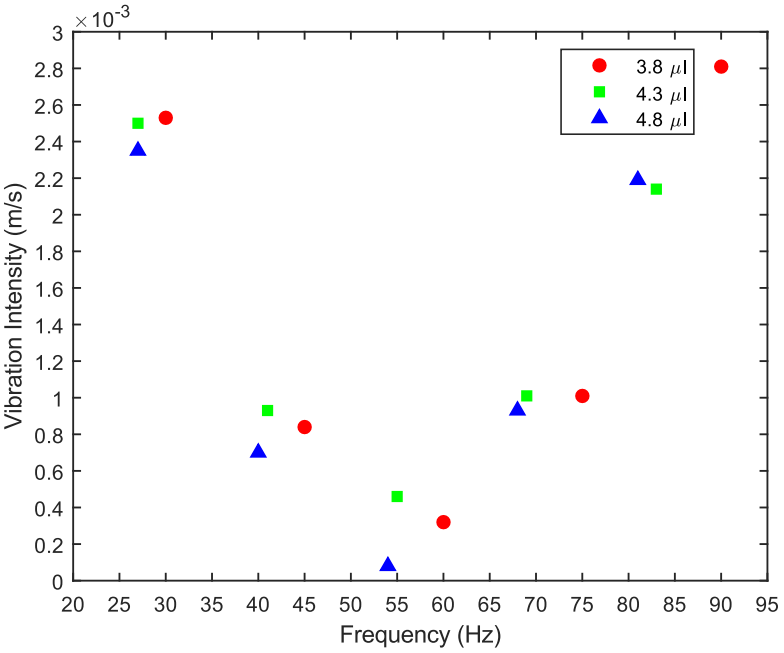

Figure 3.22: Vibration intensity vs. frequency at sliding for different droplet volumes on PTFE

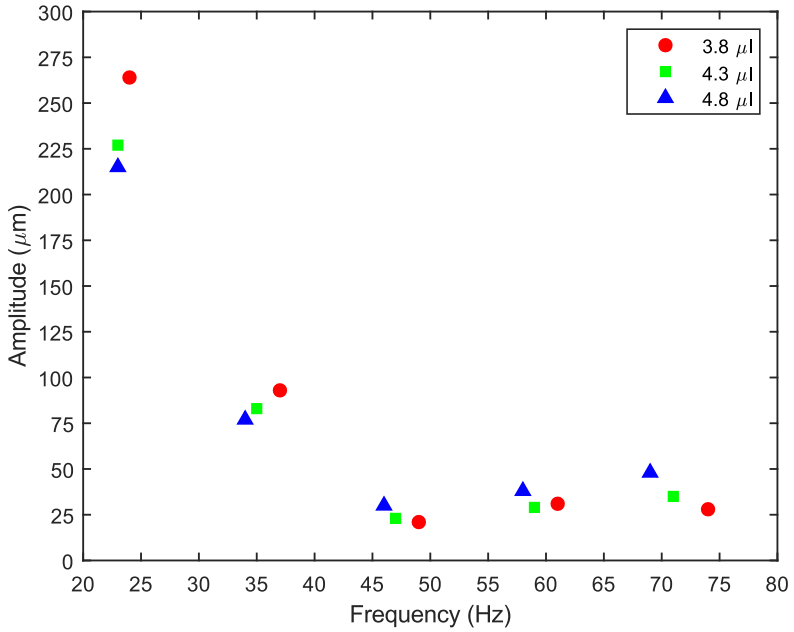

Figure 3.23: Amplitude vs. frequency at sliding for different droplet volumes on Saphir

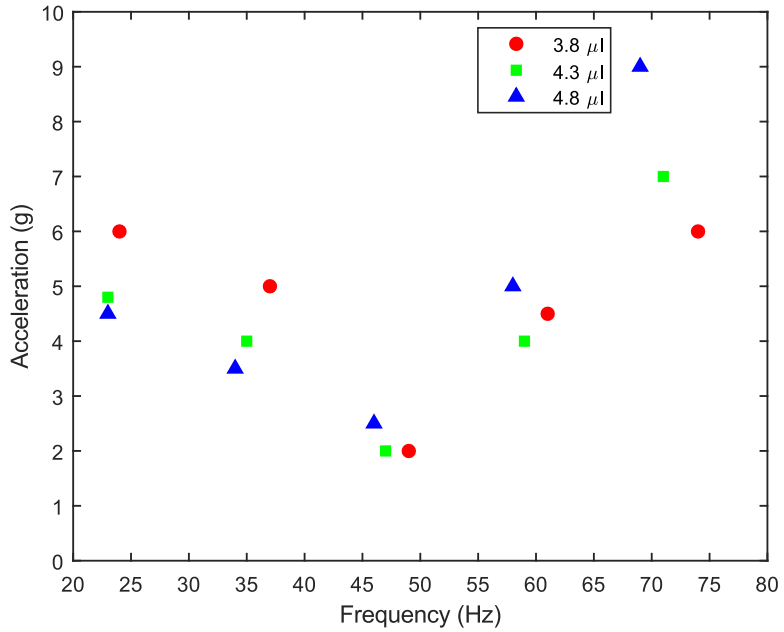

Figure 3.24: Acceleration vs. frequency at sliding for different droplet volumes on Saphir

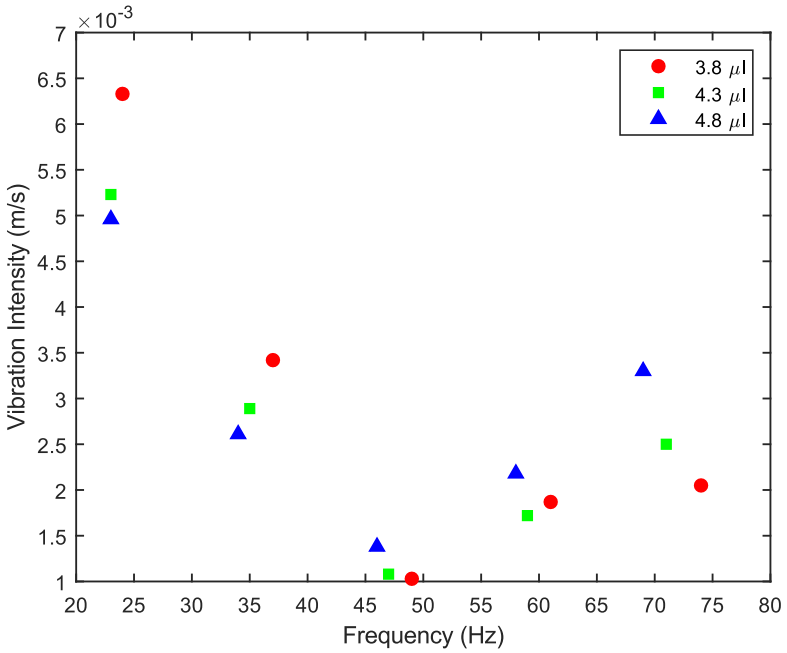

Figure 3.25: Vibration intensity vs. frequency at sliding for different droplet volumes on Saphir

From the above figures, the amplitude of vibration had to be increased with reducing droplet size or volume for sliding to occur. A similar trend was observed for acceleration and vibration intensity as well. This phenomenon can be explained by considering a force balance. When the substrate in undergoing downward motion, the inertial force and gravitational force add up. This combination of forces must overcome the adhesive force for sliding to occur. In larger droplets, the droplets can overcome this force easier, since the inertial force is dependent on the mass of the droplet. In smaller droplets, more vibration energy is required to overcome the same adhesive force, since the inertial force is now reduced relative to the contact area between the droplet and the substrate.

In summary, the results show that vibration intensity decreases with increasing droplet volume at any frequency.

3.5.2 Effect of substrate on sliding parameters

The effect of different substrates by keeping droplet size constant, was studied as well. The effects of varying the substrate on parameters like amplitude, acceleration and vibration intensity during sliding for 3.8 µl (Fig. 3.26 – 3.28), 4.3 µl (Figure 3.29 – 3.31) and 4.8 µl (Figure 3.32 – 3.33) are shown below.

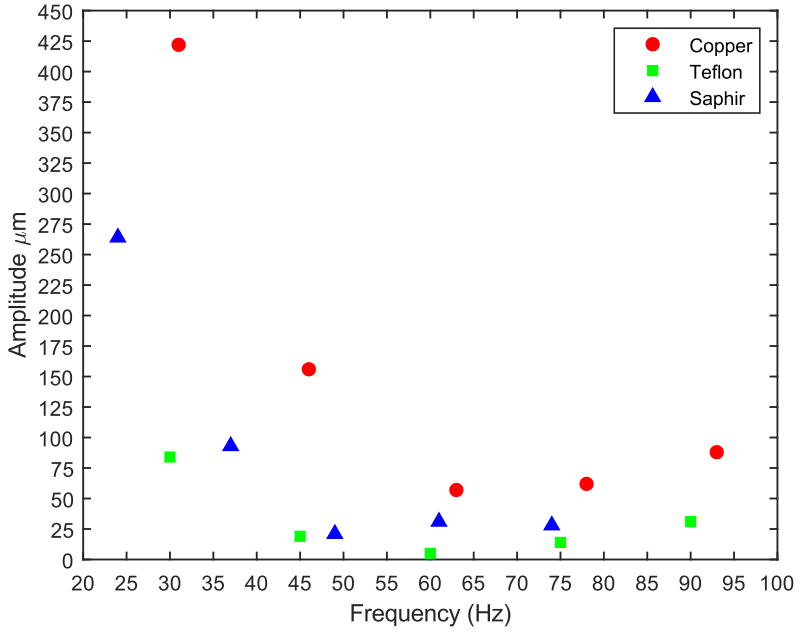

Figure 3.26: Amplitude vs. frequency at sliding for different substrates (3.8 µl droplet)

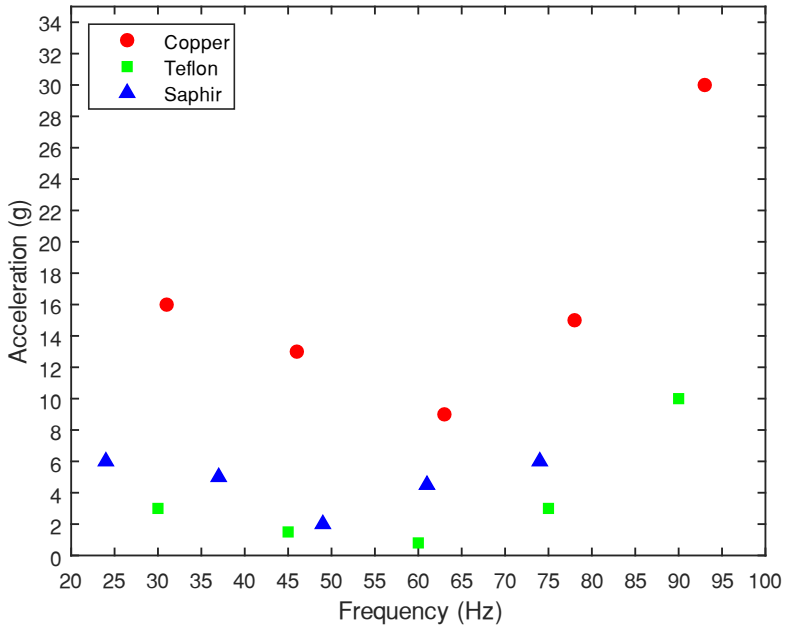

Figure 3.27: Acceleration vs. frequency at sliding for different substrates (3.8 µl droplet)

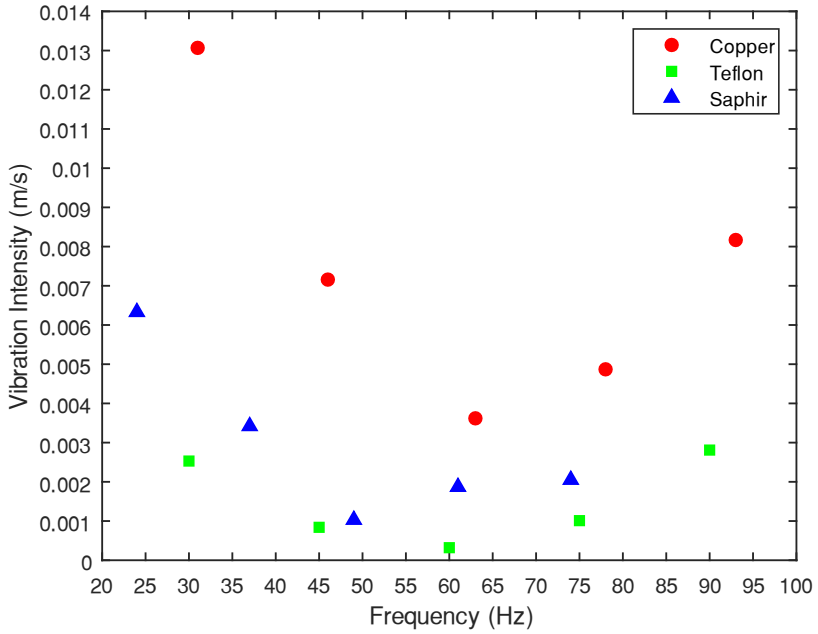

Figure 3.28: Vibration intensity vs. frequency at sliding for different substrates (3.8 µl droplet)

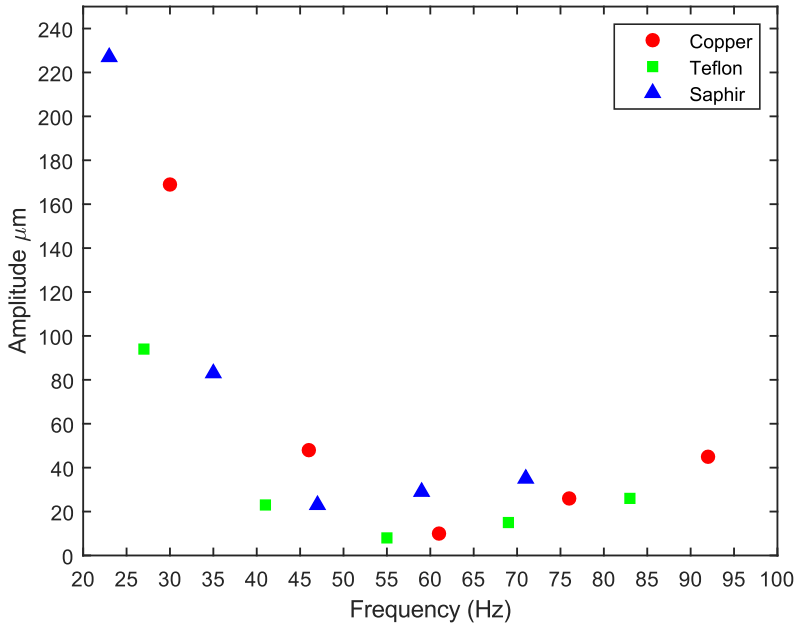

Figure 3.29: Amplitude vs. frequency at sliding for different substrates (4.3 µl droplet)

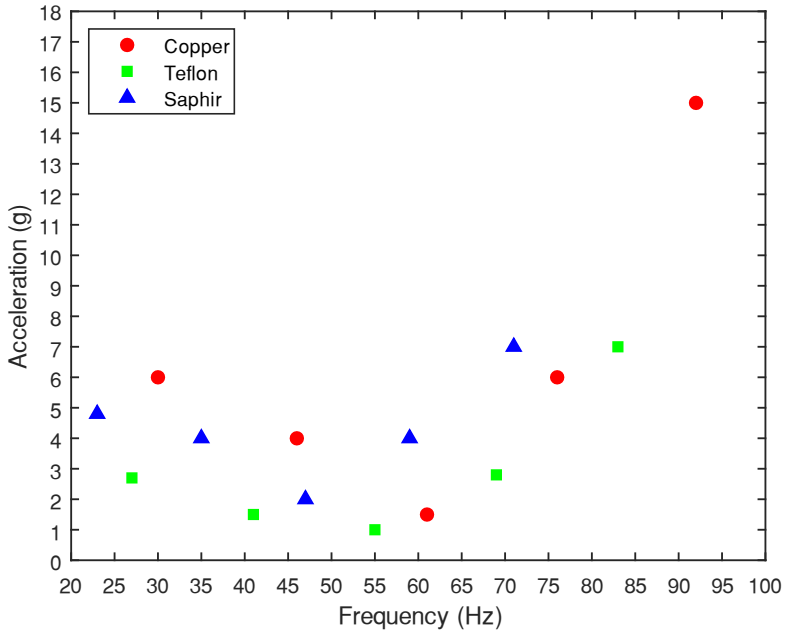

Figure 3.30: Acceleration vs. frequency at sliding for different substrates (4.3 µl droplet)

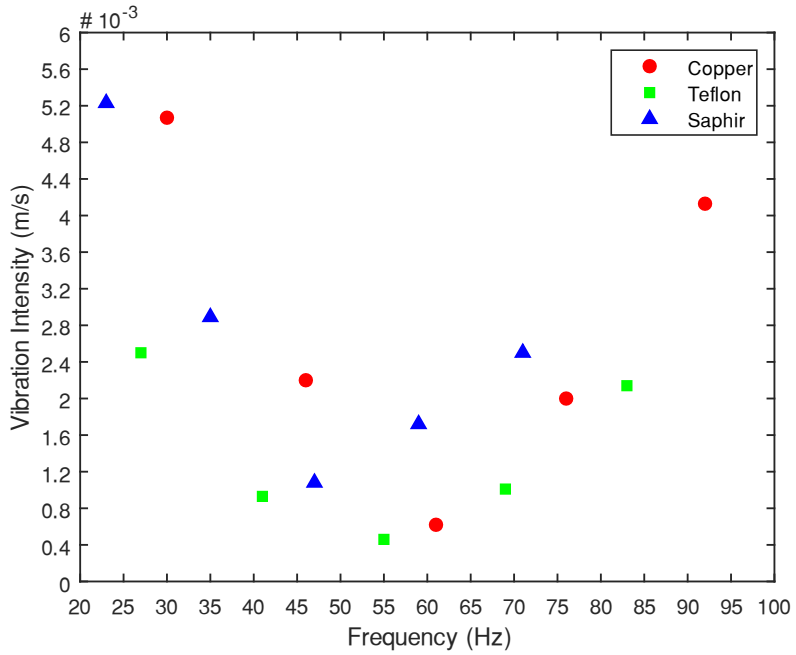

Figure 3.31: Vibration intensity vs. frequency at sliding for different substrates (4.3 µl droplet)

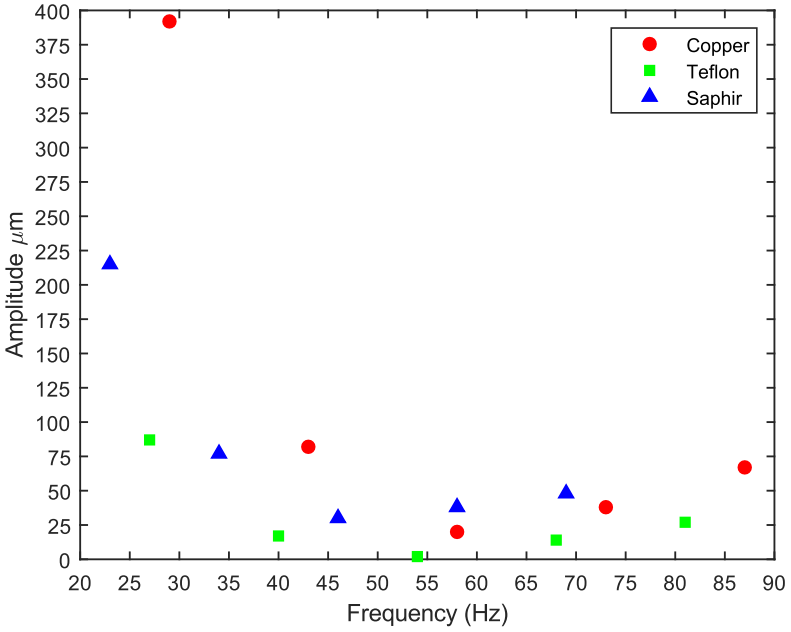

Figure 3.32: Amplitude vs. frequency at sliding for different substrates (4.8 µl droplet)

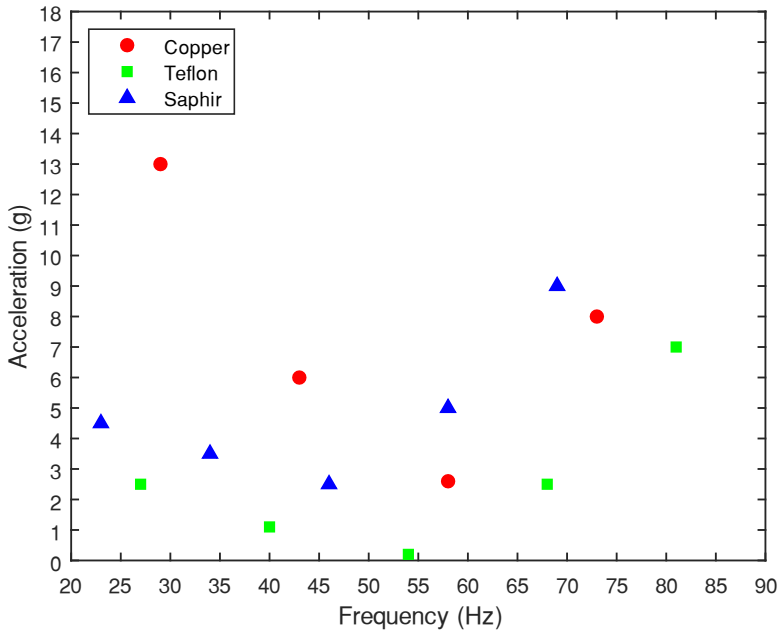

Figure 3.33: Acceleration vs. frequency at sliding for different substrates (4.8 µl droplet)

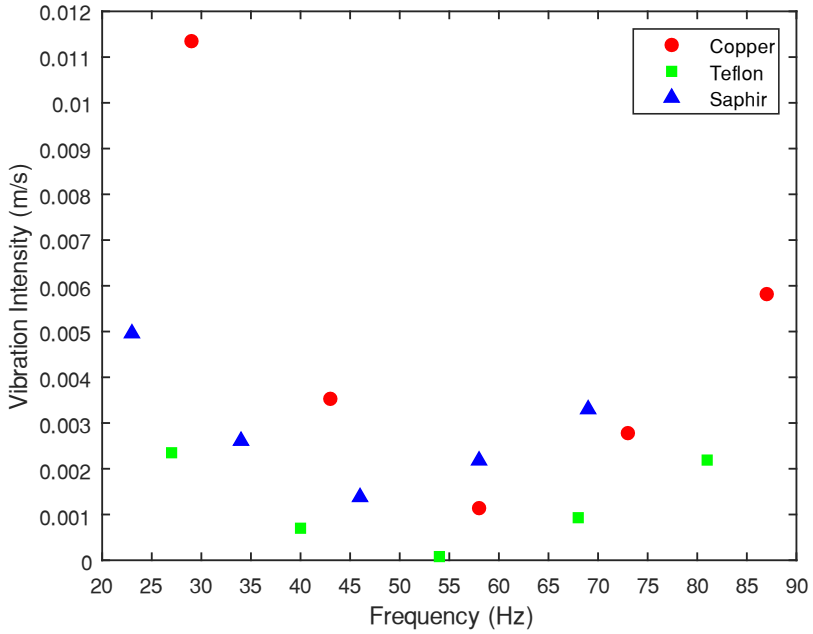

Figure 3.34: Vibration intensity vs. frequency at sliding for different substrates (4.8 µl droplet)

From figures above, it is evident that increasing hydrophobicity of the substrate aids droplet sliding. PTFE requires the least acceleration, amplitude as well as vibration intensity for droplet of the same size to slide. However, Saphir in spite of being more hydrophobic than PTFE requires more acceleration, amplitude and vibration intensity to slide compared to PTFE. This is attributed to the increased level of roughness of the substrate compared to PTFE, as shown in Figures 3.1 – 3.3 and Table 3.1. As Table 3.1 indicates, Saphir on average is about 19% rougher than PTFE. It is known that substrates with greater level of roughness result in greater adhesion forces [44]. This explains why Saphir shows greater vibration intensity than PTFE, even though Saphir is more hydrophobic.

The vibration intensity level required for droplet sliding is lower for hydrophobic substrates than for hydrophilic substrates. On hydrophobic substrates, the corresponding droplet contact angle and the droplet's center of mass are greater than on a hydrophilic substrate. This makes the droplet relatively unstable, which facilitates the sliding process.

One of the important outcomes of this study was the observed effect of resonant frequency on droplets. As Figures 3.17 – 3.32 show, resonant frequencies always require the least acceleration, amplitude and vibration intensity to promote droplet sliding. This effect was first observed by Daniel *et. al.* [36], who observed maximum velocities of droplet motion when subjected to lateral vibrations at frequencies corresponding to the first and second harmonics of the droplet. Their observations are consistent with the current study

in which parameters like amplitude, acceleration and vibration intensity are at their lowest at resonance.

In real life applications, if a condensing surface is vibrated at resonant frequencies, the acceleration required will be relatively low. However, as frequency shifts away from resonance, the acceleration would have to be increased to promote droplet shedding. This can have detrimental effects like shock and fatigue on the condensing surface and the equipment attached to it. Likewise, smooth and hydrophobic surfaces like PTFE have been proven to require lower levels of acceleration for droplets to slide. Thus, hydrophobic surfaces should be preferred to hydrophilic or rough surfaces to enable droplet sliding at lower accelerations.

Similarly, vibrational intensity has been defined as the vibrational power flow per unit width of cross sectional area [45]. Thus, it can be related directly to the vibration energy required by a system. Operating the system at resonant frequency of the droplets should lead to lower vibrational intensity required by the droplets to slide. This can lead to substantial savings in energy.

In conclusion, vibrations should be imposed at resonant frequencies to obtain superior droplet movement with the least amount of external energy.

4. CONCLUSION AND FUTURE WORK

This study deals with the effects of imposing resonant frequency on droplets for enhanced droplet sliding. The study began with characterization of the substrates and their interaction with the liquid. We tested three substrates – copper, PTFE, and Saphir. Copper was hydrophilic with a contact angle of 85.5^{o} but it had a high roughness value of 0.62 μm. PTFE and Saphir, on the other hand, were hydrophobic and had contact angles of 100.0^{o} and 115.9^{o}, respectively. They also had a roughness of 0.37 μm and 0.44 μm, respectively.

In the next phase of the study, the first resonance frequency (rocking mode) of droplets of varying volumes (3.3 μl to 6.8 μl) on three substrates were determined experimentally. Contact angle hysteresis was used as the criteria to determine resonant state. The frequencies obtained experimentally were then compared with Celestini's model and a 20 % discrepancy was observed. As the volume of the droplet increased, the resonant frequency decreased in both the cases. Similarly, for droplets at the same volume, the resonant frequency increased with static contact angle (hydrophobicity).

In the final phase of the study, the droplets were vibrated at resonant frequency as well as at ± 25% and ± 50% from the resonant frequency on all three substrates until sliding was observed. When compared between different substrates, it was observed that droplet sliding occurred relatively easily on hydrophobic substrates compared to hydrophilic substrates of similar roughness, like on copper and Saphir. This is due to the fact that droplets of the same volume deposited on a hydrophobic substrate have a higher center of

mass than ones deposited on a hydrophilic substrate. This makes the former more unstable and thus, more susceptible to slide.

However, droplets slid more easily on PTFE than on Saphir even though Saphir is more hydrophobic. This is because Saphir has a higher level of roughness compared to PTFE. The adhesion force is dependent on the contact area, which is higher for a rougher substrate. Considering more inertial force due to vibration is required to overcome this increased adhesion force, droplets slide more easily on PTFE compared to Saphir. This shows that both hydrophobicity and roughness of the substrates must be considered while conducting droplet sliding experiments.

The effect of droplet size on sliding was also observed for different substrates. In general, it was observed that droplets of larger sizes slide easily compared to droplets of smaller sizes. This is due to the fact that, while adhesion force depends on square of the droplet radius, the inertial force due to vibrations depends on cube of the droplet radius. Thus, as the droplet size increases, inertial force dominates which makes sliding easier.

Another important result from the current study was the effect of resonance on vibration parameters, such as amplitude, acceleration, and vibration intensity. It was observed that if the droplets are vibrated at resonant frequency, they tend to slide much more easily compared to other frequencies. Thus, the vibration energy spent is significantly lower at resonance. It was also observed that acceleration required for droplets to slide at resonant frequencies was much lower than at other frequencies. These trends for vibration

intensity, amplitude and acceleration were consistently observed across droplets of all volumes and on substrates of all wettabilities that were tested.

Results of this study indicate the effects of surface wettability and droplet size on droplet sliding, as well as the effects of using resonant frequencies. Initially, the three substrates were chosen on the basis of hydrophobicity, but the results from the sliding experiments also indicated the significance of roughness on droplet sliding. Thus, the effect of roughness of hydrophilic and hydrophobic substrates must be studied in greater depth.

As explained in the introductory chapter, one of the most promising applications of the current work lies in dropwise condensation. The main objective of imposing vibrations on the condensing surface is to prevent the transition of dropwise condensation to filmwise condensation. By imposing the frequency corresponding to the largest droplet sizes desired in DWC, it is possible to make droplets above that size to shed. Thus, imposing resonant vibrations could avoid film formation. This will also skew the droplet distribution favoring droplets for which resonant frequencies are higher than the imposed frequency for a given droplet size.

REFERENCES

1. Incropera, F.P. and D.P. DeWitt, *Fundamentals of heat and mass transfer*. 5th ed. ed. 2002, New York: J. Wiley.

2. Al-Shammari, S.B., D.R. Webb, and P. Heggs, *Condensation of steam with and without the presence of non-condensable gases in a vertical tube.* Desalination, 2004. 169(2): p. 151-160.

3. Fu, W., et al., *Numerical investigation of convective condensation with the presence of non-condensable gases in a vertical tube.* Nuclear Engineering and Design, 2016. 297: p. 197-207.

4. Gao, L. and T.J. McCarthy, *Contact angle hysteresis explained.* Langmuir, 2006. 22(14): p. 6234-7.

5. Navascues, G., *Liquid Surfaces - Theory of Surface-Tension.* Reports on Progress in Physics, 1979. 42(7): p. 1131-&.

6. White, L.R., *On deviations from Young's equation.* Journal of the Chemical Society, Faraday Transactions 1: Physical Chemistry in Condensed Phases, 1977. 73(0): p. 390-398.

7. Eissenberg, D.M., *Method for promoting dropwise condensation on copper and copper alloy condensing surfaces*. 1969, US Atomic Energy Commission (AEC): United States.

8. Erb, R.A. and E. Thelen, *Promoting Permanent Dropwise Condensation.* Industrial and Engineering Chemistry, 1965. 57(10): p. 49-&.

9. Das, A.K., et al., *The use of an organic self-assembled monolayer coating to promote dropwise condensation of steam on horizontal tubes.* Journal of Heat Transfer-Transactions of the Asme, 2000. 122(2): p. 278-286.

10. Torresin, D., et al., *Flow condensation on copper-based nanotextured superhydrophobic surfaces.* Langmuir, 2013. 29(2): p. 840-8.

11. Azimi, G., H.M. Kwon, and K.K. Varanasi, *Superhydrophobic surfaces by laser ablation of rare-earth oxide ceramics.* Mrs Communications, 2014. 4(3): p. 95-99.

12. Zenkin, S., S. Kos, and J. Musil, *Hydrophobicity of Thin Films of Compounds of Low-Electronegativity Metals.* Journal of the American Ceramic Society, 2014. 97(9): p. 2713-2717.

13. Qi, Z., D.C. Zhang, and J.F. Lin, *Surface Materials with Dropwise Condensation Made by Ion-Implantation Technology.* International Journal of Heat and Mass Transfer, 1991. 34(11): p. 2833-2835.

14. Preston, D.J., et al., *Heat Transfer Enhancement During Water and Hydrocarbon Condensation on Lubricant Infused Surfaces.* Sci Rep, 2018. 8(1): p. 540.

15. Preston, D.J., et al., *Scalable graphene coatings for enhanced condensation heat transfer.* Nano Lett, 2015. 15(5): p. 2902-9.

16. Didkovsky, A.B. and M.K. Bologa, *Vapor Film Condensation Heat-Transfer and Hydrodynamics under the Influence of an Electric-Field.* International Journal of Heat and Mass Transfer, 1981. 24(5): p. 811-819.

17. Laohalertdecha, S., P. Naphon, and S. Wongwises, *A review of electrohydrodynamic enhancement of heat transfer.* Renewable & Sustainable Energy Reviews, 2007. 11(5): p. 858-876.

18. Velkoff, H.R. and J.H. Miller, *Condensation of Vapor on a Vertical Plate with a Transverse Electrostatic Field.* Journal of Heat Transfer, 1965. 87(2): p. 197-&.

19. Migliaccio, C.P., *Resonance-induced condensate shedding for high-efficiency heat transfer.* International Journal of Heat and Mass Transfer, 2014. 79: p. 720-726.

20. Bejan, A. and A.D. Kraus, *Heat transfer handbook*. 2003, J. Wiley: New York.

21. Yamali, C. and H. Merte, *Influence of sweeping on dropwise condensation with varying body force and surface subcooling*, in *International Journal of Heat and Mass Transfer*. 1999, Pergamon Press: Great Britain. p. 2943.

22. United States Department of the Interior and Southwest Research Institute, *Investigation of the use of acoustic vibrations to improve heat transfer rates and reduce scaling in distillation units used for Saline water conversion*. Research and development progress report / United States Dept. of the Interior ;no. 65. 1962, Washington. D.C: U.S. Dept. of Commerce : For sale by the U.S. Dept. of Commerce, Office of Technical Services. xv, 141 p.

23. Dent, J.C., *Effect of Vibration on Condensation Heat Transfer to a Horizontal Tube.* Proceedings of the Institution of Mechanical Engineers, 2006. 184(1): p. 99-106.

24. Dent, J.C., *The calculation of heat transfer coefficient for condensation of steam on a vibrating vertical tube.* International Journal of Heat and Mass Transfer, 1969. 12(9): p. 991-996.

25. Rahimzadeh, A. and M. Eslamian, *Experimental study on the evaporation of sessile droplets excited by vertical and horizontal ultrasonic vibration.* International Journal of Heat and Mass Transfer, 2017. 114: p. 786-795.

26. Andrieu, C., C. Sykes, and F. Brochard, *Average Spreading Parameter on Heterogeneous Surfaces.* Langmuir, 1994. 10(7): p. 2077-2080.

27. Brunet, P., J. Eggers, and R.D. Deegan, *Motion of a drop driven by substrate vibrations.* European Physical Journal-Special Topics, 2009. 166(1): p. 11-14.

28. Sartori, P., et al., *Drop motion induced by vertical vibrations.* New Journal of Physics, 2015. 17(11): p. 113017.

29. Noblin, X., A. Buguin, and F. Brochard-Wyart, *Vibrated sessile drops: transition between pinned and mobile contact line oscillations.* Eur Phys J E Soft Matter, 2004. 14(4): p. 395-404.

30. Boreyko, J.B. and C.H. Chen, *Restoring superhydrophobicity of lotus leaves with vibration-induced dewetting.* Phys Rev Lett, 2009. 103(17): p. 174502.

31. Quéré, D., M.-J. Azzopardi, and L. Delattre, *Drops at Rest on a Tilted Plane.* Langmuir, 1998. 14(8): p. 2213-2216.

32. Lamb, H., *Hydrodynamics*. 1932: Cambridge University Press, UK.

33. Strani, M. and F. Sabetta, *Free-Vibrations of a Drop in Partial Contact with a Solid Support.* Journal of Fluid Mechanics, 1984. 141(Apr): p. 233-247.

34. Dong, L., A. Chaudhury, and M.K. Chaudhury, *Lateral vibration of a water drop and its motion on a vibrating surface.* Eur Phys J E Soft Matter, 2006. 21(3): p. 231-42.

35. Huber, R.A., et al., *Vibration-Enhanced Droplet Motion Modes: Simulations of Rocking, Ratcheting, Ratcheting With Breakup, and Ejection.* Journal of Fluids Engineering-Transactions of the Asme, 2019. 141(7): p. 071105.

36. Daniel, S., et al., *Ratcheting motion of liquid drops on gradient surfaces.* Langmuir, 2004. 20(10): p. 4085-92.

37. Daniel, S., M.K. Chaudhury, and P.G. de Gennes, *Vibration-actuated drop motion on surfaces for batch microfluidic processes.* Langmuir, 2005. 21(9): p. 4240-8.

38. Celestini, F. and R. Kofman, *Vibration of submillimeter-size supported droplets.* Phys Rev E Stat Nonlin Soft Matter Phys, 2006. 73(4 Pt 1): p. 041602.

39. *Online Tone Generator*. Available from: http://onlinetonegenerator.com/.

40. Stalder, A.F., et al., *A snake-based approach to accurate determination of both contact points and contact angles.* Colloids and Surfaces a-Physicochemical and Engineering Aspects, 2006. 286(1-3): p. 92-103.

41. Graham, C. and P. Griffith, *Drop Size Distributions and Heat-Transfer in Dropwise Condensation.* International Journal of Heat and Mass Transfer, 1973. 16(2): p. 337-346.

42. Leach, R.N., et al., *Dropwise Condensation: Experiments and Simulations of Nucleation and Growth of Water Drops in a Cooling System*. 2006, American Chemical Society: United States. p. 8864.

43. Rose, J.W. and L.R. Glicksman, *Dropwise condensation—The distribution of drop sizes.* International Journal of Heat and Mass Transfer, 1973. 16(2): p. 411-425.

44. Meine, K., et al., *The influence of surface roughness on the adhesion force.* Surface and Interface Analysis, 2004. 36(8): p. 694-697.

45. Noiseux, D.U., *Measurement of Power Flow in Uniform Beams and Plates.* Journal of the Acoustical Society of America, 1970. 47(1p2): p. 238-&.